KTH Chemical Science
and Engineering

An Experimental and Theoretical Study of the Mass Transport in Lithium-Ion Battery Electrolytes

Andreas Nyman

Doctoral Thesis

Applied Electrochemistry
School of Chemical Science and Engineering
Kungliga Tekniska Högskolan, 2011

Akademisk avhandling som med tillstånd av Kungliga Tekniska Högskolan i Stockholm, framlägges till offentlig granskning för avläggande av teknologie doktorsexamen måndagen den 28:e februari 2011, kl. 10.00 i sal K2, Teknikringen 28, Entréplan, Kungliga Tekniska Högskolan

Printed in Sweden
E-Print, Stockholm 2011

TRITA-CHE-Report 2011:6
ISSN 1654-1081
ISBN 978-91-7415-852-6

Abstract

Lithium-ion batteries are particularly suitable as energy storage solutions in high power applications, such as hybrid electric vehicles. It is generally considered that one of the processes that limit the power density for lithium-ion batteries is the mass transport in the electrolyte. Yet, it is still difficult to find a set of properties that fully describe the mass transport for the most common electrolytes.

In this work, characterization studies of the mass transport were undertaken for two technically important lithium-ion battery electrolytes: (1) a liquid electrolyte which consist of $LiPF_6$ dissolved in ethyl methyl carbonate (EMC) and ethylene carbonate (EC) and, (2) a gel electrolyte which consists of $LiPF_6$ dissolved in ethylene carbonate, propylene carbonate (PC) and poly(vinylidenefluoride-hexafluoropropylene) (P(VdF-HFP)).

The mass transport in the electrolytes was characterized by combining several experiments. The Maxwell-Stefan equation was used as basis for the characterization. Models of the transport were formulated from the equation and the apparent transport properties were identified. The characterization methods were first analyzed mathematically in order to establish at which conditions the characterization experiments should be performed. The values of the apparent transport properties were then obtained by optimizing the models to the experimental responses. In order to give the characterization results a comprehensible interpretation and to allow benchmarking of electrolytes, the concept of a normalized potential gradient was introduced.

The characterization results of the liquid electrolyte were used in a full cell model of a $LiNi_{0.8}Co_{0.15}Al_{0.05}O_2$ | $LiPF_6$ EC:EMC (3:7) | MAG-10 cell. The model was developed to analyze the mass transport during a hybrid pulse power characterization (HPPC) test. The analysis was made with a method where the polarization was split up into parts each associated with a process within the cell.

The optimum composition in terms of mass transport was found to lie between 0.5 and 1.2 mol/dm^3 $LiPF_6$ for the liquid electrolyte and between 5 and 7 wt. % $LiPF_6$ for the gel electrolyte. Less amount of polymer in the gel electrolyte gave a faster mass transport. It was also found that the mass transport in the liquid electrolyte contributed to a major part of the polarization during HPPC tests.

Keywords: Lithium-ion batteries, Electrolytes, Transport properties, Conductivity, Diffusion coefficients, Transport number, Maxwell-Stefan equation, Simulations, Mathematical analysis, Polarization, Hybrid electric vehicles

Sammanfattning

Litiumjonbatterier är speciellt lämpliga som ackumulatorer i högeffektsapplikationer som elhybridfordon. Det är idag allmänt accepterat att en av processerna som begränsar effekttätheten för litiumjonbatterier är masstransporten i elektrolyten. Trots detta är det fortfarande svårt att få tag på data som fullständigt beskriver masstransporten i de vanligaste elektrolyterna.

I det här arbetet har masstransportkarakteriseringar gjorts för två tekniskt viktiga elektrolyter: (1) en vätskeelektrolyt som består av $LiPF_6$ upplöst i etylenkarbonat (EC) och etylmetylkarbonat (EMC), och (2) en gel elektrolyt som består av $LiPF_6$ upplöst i EC, propylenkarbonat (PC) och poly(vinylidene fluoride-hexafluoro propylene) (P(VdF-HFP)).

Masstransporten i elektrolyterna karakteriserades genom att kombinera ett antal karakteriseringsexperiment. Maxwell-Stefans ekvation användes som utgångspunkt i karakteriseringarna. Modeller av transporten formulerades från ekvationen och de effektiva transportegenskaperna identifierades. En matematisk analys gjordes först av karakteriseringstekniken, så att det kunde fastslås för vilka förhållanden experimenten skulle utföras. Värderna av transportegenskaperna erhölls genom att optimera modellerna till det experimentella beteendet. För att ge karakteriseringsresultaten en begriplig tolkning och för att kunna mäta prestandan av elektrolyter, infördes konceptet normaliserad potentialgradient.

Resultatet från karakteriseringen av vätskeelektrolyten användes i en model av en $LiNi_{0.8}Co_{0.15}Al_{0.05}O_2$ | $LiPF_6$ EC:EMC (3:7) | MAG-10 cell. Modellen utvecklades för att analysera masstransporten i cellen under ett hybridpulstest (HPPC). Analysen gjordes med en metod där polarisationen delades upp i delar som var och en var kopplad till en process i batteriet.

Den optimala sammansättningen med avseende på masstransporten låg i regionen 0.5–1.2 mol/dm^3 $LiPF_6$ för vätskeelektrolyten och 5-7 vikt% $LiPF_6$ för gelelektrolyten. Mindre mängd polymer i gelelektrolyten gav en snabbare masstransport. Det konstaterades också att masstransporten i vätskeelektrolyten bidrog med en av de största delarna till polarisationen i HPPC testen.

Nyckelord: Litiumjonbatterier, Aprotiska elektrolyter, Transport egenskaper, Konduktivitet, Diffusion koefficienter, Transporttal, Maxwell-Stefans ekvation, Simuleringar, Matematisk analys, Polarisation, Hybridfordon

List of Papers

I. Electrochemical characterisation and modelling of the mass transport phenomena in $LiPF_6$-EC-EMC.
A. Nyman, M. Behm and G. Lindbergh.
Electrochimica Acta, **53**, *6356-6365 (2008).*

II. Analysis of the polarization in a Li-ion battery cell by numerical simulations.
A. Nyman, T. G. Zavalis, R. Elger, M. Behm and G. Lindbergh.
Journal of the Electrochemical Society, **157** *(11), A1236-A1246 (2010).*

III. A theoretical and experimental study of the mass transport in gel electrolytes. 1. Mathematical analysis of characterization method.
A. Nyman, M. Behm and G. Lindbergh.
Manuscript under revision after peer review in the Journal of the Electrochemical Society.

IV. A theoretical and experimental study of the mass transport in gel electrolytes. 2. Experimental Characterization of $LiPF_6$-EC-PC-P(VdF-HFP).
A. Nyman, M. Behm and G. Lindbergh.
Manuscript under revision after peer review in the Journal of the Electrochemical Society.

The modelling in paper II was made together with Tommy Zavalis. The experiments were performed by Ragna Elger. The work in the rest of the papers was performed by me.

Contents

Chapter 1 Introduction 1
1.1 The Lithium-Ion Battery 1
1.2 Electrolytes in Lithium-ion Batteries 3
1.3 Mass Transport in Electrolytes 4
1.4 Mass Transport Characterization of Electrolytes 6
1.5 Aim of the Thesis 8
Chapter 2 Experimental 9
2.1 Sample Preparations 9
2.2 Conductivity Measurements 10
2.3 Concentration Cells 11
2.4 Galvanostatic Polarization Experiments 11
2.5 Diffusion Experiments 12
Chapter 3 Macroscopic Modelling of the Mass Transport in Electrolytes 13
3.1 Maxwell-Stefan Equation for Electrolytes 13
3.2 Transport Properties for $LiPF_6$ dissolved in EC and EMC 16
3.3 Transport Properties for $LiPF_6$ dissolved in EC, PC and P(VdF-HFP) 17
3.4 Electrolyte Mass Transport in Separators and Porous Electrodes 18
3.5 Macroscopic Modelling of Characterization Experiments 19
3.6 Macroscopic Modelling of a Li-Ion Cell during HPPC-tests 20
Chapter 4 Extraction of Transport Properties from Characterization Experiments 25
4.1 Conductivity measurements 25
4.2 Concentration Cells 25
4.3 Extraction of Diffusion Coefficients and Transport Numbers 26
Chapter 5 Characterization Results and Implications 35
5.1 The Mass Transport in the Liquid Electrolyte: $LiPF_6$-EC-EMC 35
5.2 The Mass Transport in the Gel Electrolyte: $LiPF_6$-EC-PC-P(VdF-HFP) 39
5.3 Polarization due to the Mass Transport in a Battery Cell 44
5.4 Benchmarking of Electrolytes 48
Chapter 6 Conclusions 53

List of Symbols 57
Acknowledgements 61
References 63

Chapter 1

Introduction

Rechargeable batteries are being used today in many products in our society. Even though the market for rechargeable batteries is changing yearly due to the development of several new applications, four of the most common batteries are the same: lead-acid, nickel metal hydride, nickel cadmium and lithium-ion batteries. This thesis is devoted to the latter one. The lithium-ion battery was first introduced as a commercial battery by Sony in 1990 (1). It has the advantage of having higher gravimetric and volumetric energy densities, lower self-discharge rate and higher voltage output compared to the other battery chemistries, which makes it particularly suitable for portable devices and vehicles. It is expected that the market for lithium-ion batteries will grow as the production rate of hybrid electric and electric vehicles will increase. In 2007, the value of the lithium-ion battery market was approximately 2.4 billion USD in the United States of America. It is predicted that the value will be 3.7 billion USD in 2012 (2).

1.1 The Lithium-Ion Battery

A lithium-ion battery consists of two electrodes with a separator in between. The total thickness of the assembly is approximately 70-200 μm, depending on the type of application the cell is intended for. Battery cells are assembled by winding or stacking the layers of the electrodes and the separator into cylindrical or prismatic shapes. The electrode with the highest electrode potential is called the positive electrode. It usually consists of a transition metal material, which can host lithium ions. The other electrode is usually made of graphite and it is called the negative electrode. Both the electrodes and the separator are porous. An electrolyte fills up the pores to create electrolytic contact between the electrodes. The electrolyte is a lithium salt dissolved in a mixture of solvents, polymers or ionic liquids. The process is represented by the reactions below, where X represents the transition metal material in the positive electrode and C_6 the graphite in the negative electrode:

$$Li_yC_6 \rightleftharpoons yLi^+ + ye^- + C_6 \qquad \text{Negative electrode}$$

$Li_xX + zLi^+ + ze^- \rightleftharpoons Li_{x+z}X$ Positive electrode

The electrons that are produced during the oxidation travel through an external circuit to the other electrode where they are consumed in the reduction.

Tabel 1.1: *Cell chemistry of a lithium-ion cylindrical 18650 cell designed for hybrid electric vehicle use with a total capacity of 0.9 Ah.*

Negative	92 wt % MAG-10 graphite, 8 wt % PVDF binder
	5 mg cm^{-2} active loading density
	Porous electrode thickness 35 µm
	Current collector of copper
Positive	84 wt % $LiNi_{0.8}Co_{0.15}Al_{0.05}O_2$, 8 wt % PVDF binder, 4 wt % SFG-6 graphite, 8 wt % carbon black
	8 mg cm^{-2} active loading density
	Porous electrode thickness 35 µm
	Current collector of aluminium
Separator	Celgard 2325 PP/PE/PP
	Separator thickness 25 µm
Electrolyte	1.2 mol/dm^3 $LiPF_6$ EC:EMC (3:7 by weight)

An example of a lithium-ion cell chemistry is presented in table 1.1. The cell is a 18650 type cylindrical cell for hybrid electric vehicle use with a capacity of 0.9 Ah. The active material that hosts the lithium ions in the negative electrode is MAG-10 graphite and for the positive electrode it is $LiNi_{0.8}Co_{0.15}Al_{0.05}O_2$. The active material is mixed with a polymer binder to enhance the mechanical stability and if the active material is a poor conductor a conducting material is added to improve the electronic conductivity. The mixture is placed on a metal foil to support the electrode material and to act as a current collector. Aluminium is used for the positive electrode, while copper is used for the negative electrode. The separator, which is placed between the two electrodes to prevent short circuit of the cell, is a three-layer Celgard separator, made of polypropylene (PP) and polyethylene (PE). The electrolyte consists of lithium hexafluorophosphate which is dissolved in a mixture of ethylene carbonate (EC) and ethyl methyl carbonate (EMC).

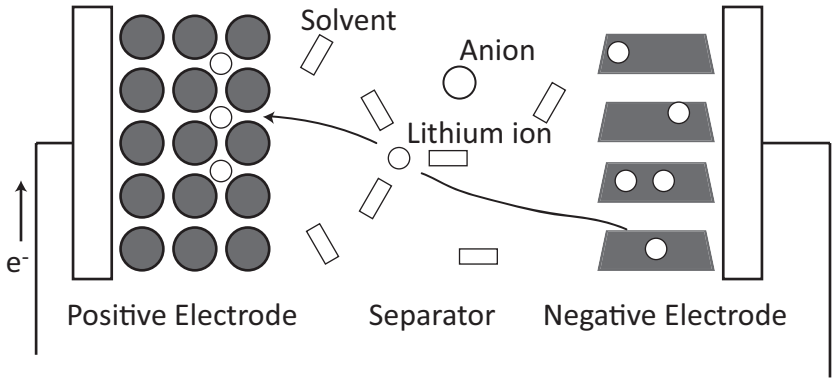

Figure 1.1: *Schematic figure of a cell.*

During discharge, lithium ions deintercalate into the electrolyte from the negative electrode. At the same time, lithium ions intercalate into the positive electrode from the electrolyte. It can therefore be said that lithium ions are moved from the negative electrode to the positive electrode during discharge (see figure 1.1). The process is reversed during charging.

1.2 Electrolytes in Lithium-ion Batteries

For the cell described in table 1.1, the amount of lithium ions that needs to be transferred from the 9 dm^2 large negative electrode to the positive electrode is approximately 0.033 mol Li^+. This value can be compared to how much lithium that can be found in the electrolyte, which is 0.0033 mol Li^+. The lithium ions in the electrolyte are exchanged 10 times when the cell is completely discharged. Most of the lithium ions are deintercalated and transported through the separator where they are intercalated. The transport of the lithium ions in the electrolyte plays therefore an important role in the working principles of the battery. This is also illustrated in the thickness of the electrodes in commercial lithium-ion battery cells. They are usually between 20-100 μm, which can be compared to the electrodes in a lead-acid battery that are usually a couple of millimetres. The reason for the thinner electrodes is that organic electrolytes are used in lithium-ion cells, due to the high operating voltage, and they are usually worse ionic conductors than water electrolytes. This leads to mass transport limitations, which can be reduced by making the electrodes and the separator thinner. However, they cannot be made infinitely small since the energy density would then drop drastically. The mass transport in the electrolyte is therefore one of the processes that limits the power that can be drawn from lithium-ion battery cells.

The four most common types of electrolytes that are used in lithium-ion batteries are, ionic liquids, solid polymer electrolytes, gel electrolytes and organic liquid electrolytes and they are listed in table 1.2 with their properties.

Tabel 1.2: *Properties of different kinds of electrolytes used in lithium-ion batteries*

Electrolyte	Electrochemically stable	Mass transfer	Safe
Ionic Liquids	+	-	+
Solid polymer	+/-	-	+
Gel electrolytes	+/-	+	-
Organic liquid electrolytes	+/-	+	-

As mentioned before, the main role of the electrolytes in batteries is to serve as the medium for the transfer of ions between a pair of electrodes. In order to do so, the electrolyte has to be electrochemically stable, facilitate a fast mass transfer of the lithium ions, be inert to other cell components and be safe (3). Ionic liquids and solid polymer electrolytes have low vapour pressures and good thermal stability and are also

non-flammable. The ionic liquids also have a high oxidation potential. They are therefore good electrolytes in terms of safety. However, they have a large drawback since their conductivity is low at room temperature (4, 5). They are therefore not found in commercial cells. A way to solve the problem with the low conductivity is to add a solvent to a solid polymer electrolyte. This type of electrolyte is usually called a gel electrolyte. It can be found in commercial cells called Li-Poly. These electrolytes usually have a higher conductivity and even if they contain a solvent the vapour pressure is still low, which is good for safety reasons (6). The other type of electrolyte that can be found in commercial battery cells is the liquid electrolyte. They have a relatively high conductivity. However, they are highly flammable which can lead to safety hazards (5).

In this thesis, the mass transport in two electrolytes is studied namely (1) lithium hexafluorophosphate ($LiPF_6$) dissolved in ethyl methyl carbonate (EMC) and ethylene carbonate (EC) and (2) $LiPF_6$ dissolved in EC, propylene carbonate (PC) and poly(vinylidenefluoride-hexafluoropropylene) (P(VdF-HFP)). The first one is a liquid electrolyte while the second one is a gel electrolyte. Both electrolytes are technically important. The chosen liquid electrolyte has been described by Zhang *et al.* (7) as a good electrolyte while the chosen gel electrolyte has been described by Nishi (6) as a good gel electrolyte. $LiPF_6$ dissolved in EC and EMC was also the chosen electrolyte for the Generation 2 battery technology for hybrid electric vehicles in the Freedom Car Programme (USA).

1.3 Mass Transport in Electrolytes

Ions in an electrolyte can be transported by both migration and diffusion (figure 1.2). In the beginning of a discharge of a cell, lithium ions are transported by migration from the negative to the positive electrode, due to an ohmic potential difference over the electrolyte. This potential difference causes a migration of the anions in the opposite direction and creates thus a concentration difference over the electrolyte, since the anions are not reacting at the electrodes. The concentration difference gives rise to an additional potential difference that is called the diffusion potential and a diffusion flux of the lithium ions and the anions. The diffusion potential will continue to increase until the diffusion flux is the same magnitude as the migration flux of the anions. The magnitudes of the fluxes that are created are dependent on the friction forces the species experience. For example, small concentration differences are created in an electrolyte where the anions are close to immobilized. On the other hand, if the anions experience less friction forces than the lithium ions, large concentration differences are created.

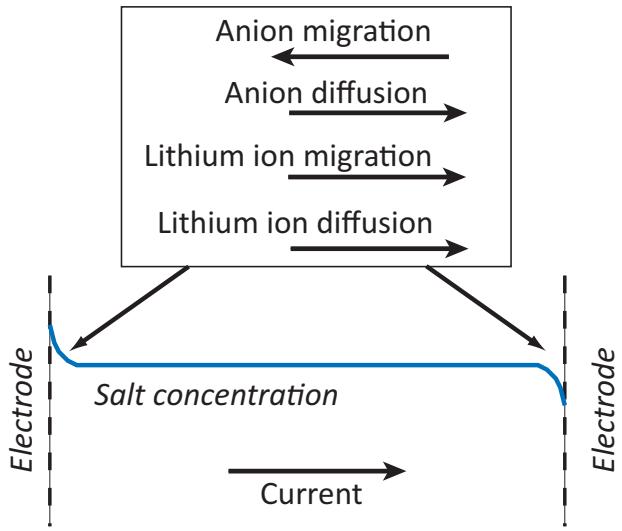

Figure 1.2: *Schematic view of the mass transport in the electrolyte*

To describe the concentration differences that appear in the electrolyte, we need to describe and quantify the friction forces. They can be described by the Maxwell-Stefan equation (eq. 1.1).

$$F_i = \sum_j K_{ij}\left(v_j - v_i\right) \tag{1.1}$$

The equation states that the driving force for the mass transport of one specie, F_i, is equal to the sum of all the friction forces that are exerted on that specie. The friction force between two species is proportional to the difference in velocity between them. From a macroscopic point of view, the friction forces are quantified by transport properties that the proportionality factors, K_{ij}, can be calculated from. There exist *n*(n-1)/2* independent mass transport properties (8), where *n* is the number of species in the electrolyte. Thus, the number of transport properties and the complexity of the mass transport are drastically increased when the number of species is increased. For a salt dissolved in one solvent, three transport properties can be defined. For a salt dissolved in a solvent and a polymer, six independent transport properties describe the mass transport.

Conventionally the transport properties are the conductivity, a set of diffusion coefficients and one or several transport numbers. However, it is possible to define and use other transport properties as well, such as Kirkwood friction parameters or Maxwell-Stefan diffusivities that are found in the Maxwell-Stefan equation. Besides the transport properties, any deviations from ideality affect the mass transport as well. Non-idealities in the electrolyte are accounted for in thermodynamic enhancement factors. Sometimes they are grouped together with the transport properties to get apparent transport properties, even if the factor is a thermodynamic property and not a strict transport property. The mass transport of the species in electrolytes are then described by *(n-1)*(n-1)* independent apparent transport properties.

The Nernst-Planck equation is often used as a description of mass transport in electrolytes. One form of the equation is written in eq. 1.2 (8).

$$\frac{\partial c_S}{\partial t} = \frac{2D_+D_-}{D_+ + D_-}\frac{\partial^2 c_S}{\partial x^2} + \frac{D_-}{D_+ + D_-}\frac{1}{F}\frac{\partial i}{\partial x} \tag{1.2}$$

According to the equation, there exist only two independent transport properties (D_+ and D_-). The transport properties can be calculated from the proportionality factors in eq. 1.1 for diluted electrolytes. However, the equation does not take into account non-idealities and the friction forces between ions. Both of these effects have shown to be important for lithium-ion battery electrolytes (9), which make it preferable to use the Maxwell-Stefan equation as the starting point for modelling instead.

1.4 Mass Transport Characterization of Electrolytes

The aim of a mass transport characterization is to obtain the values of one or several transport properties as a function of temperature or composition. The results from these characterizations are often used to compare different electrolytes to each other or to find an optimum composition. The results are also used as input data in simulations of full cells. In order to completely characterize an electrolyte, that is obtaining the values of all the transport properties (i.e. *(n-1)*(n-1)* properties), several experiments must be combined.

In the literature, mass transport characterizations of electrolytes with both electrochemical and non-electrochemical techniques can be found. The non-electrochemical techniques can be used for measurements of the diffusion coefficients, while some electrochemical techniques must be performed to measure all the other transport properties. Examples of non-electrochemical techniques are pulsed-field gradient NMR (10-14), Moiré Pattern (15) and UV/vis absorption spectroscopy (16). Examples of electrochemical techniques are the Hittorf method (17, 18), potentiostatic polarization (19-21), concentration cells (22, 23), galvanostatic polarization (22, 24, 25) and electrochemical impedance spectroscopy (26, 27). Electrochemical methods have the advantage that the experiments resemble the relevant processes occurring in a battery during use, and that the only instrumentation needed is a potentiostat. However, one has to deal with the fact that only the potential difference between two electrodes is measured, and not the concentration. This can be partly solved by relating the potential difference of the electrodes to concentration difference with concentration cell experiments. Sometimes electrochemical techniques are combined with other techniques such as in in-situ confocal Raman spectroscopy (28) and electrophoretic NMR (29, 30).

In most of the characterizations, the salt diffusion coefficient is usually estimated from the relaxation of a concentration profile. This technique was originally applied with optical detection methods; Newman and Chapman (24) observed the concentration profiles in aqueous potassium chloride under conditions of restricted diffusion by Rayleigh interference optics. They concluded that the experiment yielded a well-defined,

differential diffusion coefficient even in concentrated solutions. Ma *et al.* (31) developed this method to an electrochemical method by assuming that the quasi-electrostatic potential difference between two electrodes is proportional to the salt concentration difference when no current is passing through the cell. The concentration difference was created by galvanostatic polarization. By combining this experiment with a similar experiment under semi-infinite diffusion conditions, concentration cells and conductivity measurements a full set of thermodynamic and transport properties was determined for a sodium salt in poly(ethylene oxide).

Hafezi and Newman (32) analysed the semi-infinite galvanostatic polarization method by measurements with aqueous silver nitrate solutions. They found that at very short times after current interruption the potential difference is dominated by the double-layer capacitance and other possible surface phenomena and is not an accurate measure of concentration difference. They also suggested that the discrepancy between their model predictions and experiments at slightly longer times could be attributed to variation in the properties due to the concentration variation in the cell. It was pointed out that the galvanostatic polarization method is primarily suited for use with polymer rather than liquid electrolytes, since the required semi-infinite diffusion condition is more easily provided in polymer films where convection problems are absent. The galvanostatic polarization method was further developed by Georén and Lindbergh who determined a complete set of ionic transport properties and thermodynamic enhancement factor of a solid polymer electrolyte system (25) and $LiClO_4$ dissolved in PC (33), respectively. A galvanostatic polarization experiment was combined with conductivity measurements and concentration cells, that is, one set of experiments less than earlier methods. Numerical solution of the model equations, and optimisation of the parameters to the experimental data made it possible not to require semi-infinite diffusion in the galvanostatic experiment. This allowed concentration-dependent parameters in the model, and use of a considerably shorter cell also for the liquid electrolyte. The main problems with liquid electrolytes brought up by Hafezi and Newman were thus overcome. In a subsequent paper the model and parameters for the SPE were used to simulate concentration profiles that were experimentally confirmed with in-situ Raman spectroscopy (28). The concentration dependence of the salt diffusion coefficient for $LiClO_4$ dissolved in PC has also been obtained with Moiré Pattern by Nishikawa *et al.* (15) . Similar values as in the study of Georén and Lindbergh were reported.

Valøen and Reimers determined the complete set of transport and thermodynamic properties of $LiPF_6$–EC–PC–DMC (22). The methodology was similar to that of Ma *et al.* with the exception that a Hittorf experiment replaced the restricted diffusion experiment. The lithium ion transport number was determined from the Hittorf experiments while the ratio between the lithium ion transport number and the square root of the diffusion coefficient was measured with the semi-infinite galvanostatic polarization method. The salt activity coefficient was obtained from concentration cells. Another way to measure the salt activity coefficient is to perform melting-point-depression experiments. Stewart and Newman did that for $LiPF_6$ dissolved in EC (34). They concluded that the thermodynamic enhancement factor varies significantly with the salt concentration.

Most of the work done in the field of complete mass transport characterizations of electrolytes has been performed for liquid and solid polymer electrolytes. Measurements of the conductivity and the lithium ion transport number of gel electrolytes (21, 35, 36) can be found in the literature. But, only one complete characterization of a gel electrolyte has been reported. In that work, the system poly(methyl methacrylate) (PMMA), propylene carbonate (PC) and lithium perchlorate ($LiClO_4$) was modelled and characterized at various compositions (37). Due to the large number of transport properties that needed to be obtained, the characterization method involved both electrochemical and other experimental techniques.

1.5 Aim of the Thesis

The methods for a full characterization are still time-consuming and experimentally difficult, and the factors affecting the accuracy are not well understood. As a consequence such investigations are rarely undertaken and published despite their importance. The aim of this thesis is both to study the properties of technically important electrolyte systems and to contribute to the further development of characterization methods, exploring its possibilities and limitations. The aim is also to illustrate the importance of mass transport in lithium-ion battery cells.

Chapter 2

Experimental

Experiments were done for characterization of the liquid and the gel electrolyte. All preparation of samples and characterization experiments were carried out in a glove box filled with dry argon. The electrochemical experiments were run with a Gamry PCI4/750 potentiostat except for the conductivity measurement of the liquid electrolyte that was conducted with a Consort K912 conductometer.

2.1 Sample Preparations

The liquid electrolyte was prepared by dissolving lithium hexafluorophosphate ($LiPF_6$, Strem Chemicals, max 20 ppm water) in an ethylene carbonate and ethyl methyl carbonate mixture (EC-EMC, Quallion, 3:7 by weight). In total, 8 samples were made where the salt concentrations varied from 0.2 mol/dm^3 to 2.2 mol/dm^3. The solvent was stored over molecular sieves in order to remove residual water traces.

Table 2.1: *Composition of the characterized gel electrolytes*

Sample	$LiPF_6$		EC:PC		P(VdF-HFP)	
	weight-%	*mol/dm^3*	*weight-%*	*mol/dm^3*	*weight-%*	*mol/dm^3*
1	1	0.10	59	10.05	40	9.91
2	1	0.10	54	9.19	45	11.15
3	1	0.10	49	8.34	50	12.39
4	5	0.52	60	10.2	35	8.67
5	5	0.52	55	9.36	40	9.91
6	5	0.52	50	8.51	45	11.15
7	9	0.94	56	9.53	35	8.67
8	9	0.94	51	8.68	40	9.91
9	9	0.94	46	7.83	45	11.15

The gel electrolytes were prepared with the solvent casting technique. Nine samples of varying composition were prepared and characterized. Their compositions are shown in

table 2.1. Only mechanically stable, homogenous and phase-stable films were used in the experiments, which limited the composition range of the samples.

The salt, lithium hexafluorophosphate ($LiPF_6$, Strem Chemicals, max 20 ppm water), and the ethylene carbonate and the propylene carbonate mixture (EC:PC, 6:4 by weight, Merck, Battery Grade) were mixed with an excess of a volatile solvent. DMC (dimethyl carbonate, Merck, Battery Grade) was used as the volatile solvent, due to its high vapour pressure and low water content. Poly(vinylidenefluoride-hexafluoropropylene) (P(VdF-HFP)) was added to the solution under stirring. The homogenous solution was poured onto a Teflon sheet and the volatile solvent was allowed to vaporize for 30 hours. A freestanding film (figure 2.1) was formed, from which circular discs were cut.

Figure 2.1: *Photo of the freestanding film that was formed from the electrolyte solution*

The diameter of the discs was 1 or 1.2 cm, while the thickness varied between 400 and 1470 μm. The thickness was measured with a micrometer screw and the weight of the disc was measured with a common laboratory balance, from which the density could be calculated. The polymer used in this study is known as Kynar Flex 2801 (Atochem). It contains 12 wt% of hexafluoropropylene randomly incorporated into the vinylidenefluoride backbone. The polymer was dried for at least 48 hours before use.

2.2 Conductivity Measurements

The conductivity of the liquid electrolytes was measured with a Consort K912 conductometer with a four-electrode glass/platinum probe. The conductometer was calibrated with potassium chloride solutions outside the glove box before use to calculate the cell constant of the set up. The temperature of the electrolyte during the conductivity measurement was also measured with the conductometer to assure an electrolyte temperature of 25 ± 1 °C. The conductivity was measured five times at two different occasions for each electrolyte concentration.

The conductivity of the gel electrolyte was measured using electrochemical impedance spectroscopy (EIS). The gel was placed between two blocking-electrodes in a Swagelok cell (38). Blocking electrodes of stainless steel were used. The thickness of the

electrolyte was measured before and after the EIS measurement, to assure a constant thickness. The ionic conductivity was calculated from the x-axis intercept of the high frequency spur in the Nyquist plot.

2.3 Concentration Cells

The difference in the lithium-ion electrochemical potential between two electrolyte solutions with different composition was measured in a concentration cell with lithium foil electrodes. The concentration cell (figure 2.2) was built by placing two lithium electrodes on a microscope slide (76x26 mm). For the liquid electrolyte, a strip of glass micro fibre filter (50x10 mm) was placed on the slide to connect the two electrodes. The two electrolyte solutions were allowed to soak into the filter at its respective ends. A sufficient amount of electrolyte was added so that the two solutions would meet at midpoint, thus creating electrolytic contact in the cell.

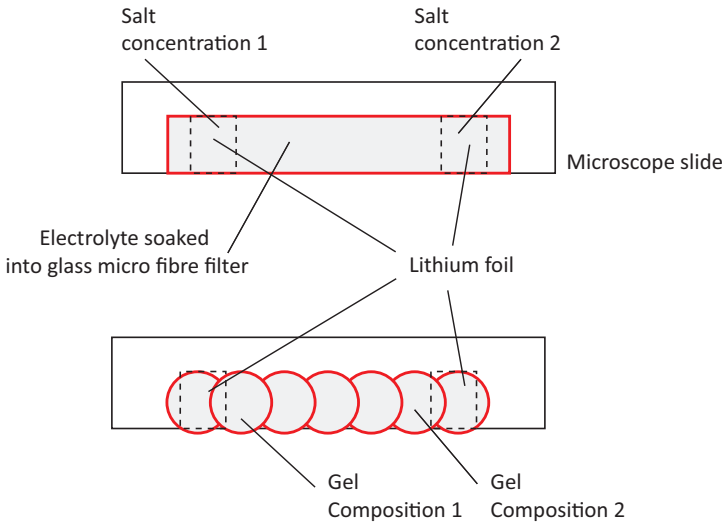

Figure 2.2: *Experimental setup of the concentration cell. Top: for a liquid electrolyte and bottom: for a gel electrolyte*

The electrolytic contact in the gel experiment was created by placing circular discs of the gel between the electrodes. The two different compositions of the gel were placed on different sides of the slide. The electrolytic contact was assured during the whole experiment by pressing another microscope slide on top of the cell.

The open circuit voltage was measured for ten minutes, so that it would stabilize. A matrix of experiments was made where the lithium-ion electrochemical potential in all electrolytes were measured against each other.

2.4 Galvanostatic Polarization Experiments

In the galvanostatic polarization experiment, the electrolyte was placed in a cell with two lithium electrodes. The cell was then polarized with constant current, which created local changes in the composition. These changes caused an added potential difference over the electrolyte, called the diffusion potential. After the current was switched off, the composition in the electrolyte was equalized by diffusion and thus the diffusion

potential relaxed. In the experiments, the relaxation of the diffusion potential was measured as a function of time.

The experiments were run in a cylindrical cell (figure 2.3). Two circular electrodes were cut from lithium foil and placed on the current collectors. For the liquid electrolyte experiments, a specified volume of electrolyte was soaked into several glass micro fibre filters (Whatman GF/A, porosity around 0.9, 1 cm diameter) to prevent leakage and convection, and placed between the electrodes in a Teflon ring (w: 500 µm id: 1.4 cm), to assure a constant length of the cell. The Bruggeman coefficient, β, of the glass micro fibre filter was estimated to 3.44 in paper I.

For the gel electrolyte experiments, the gel was placed between the lithium foils without a ring. The thickness of the gel electrolyte was measured before and after the experiment.

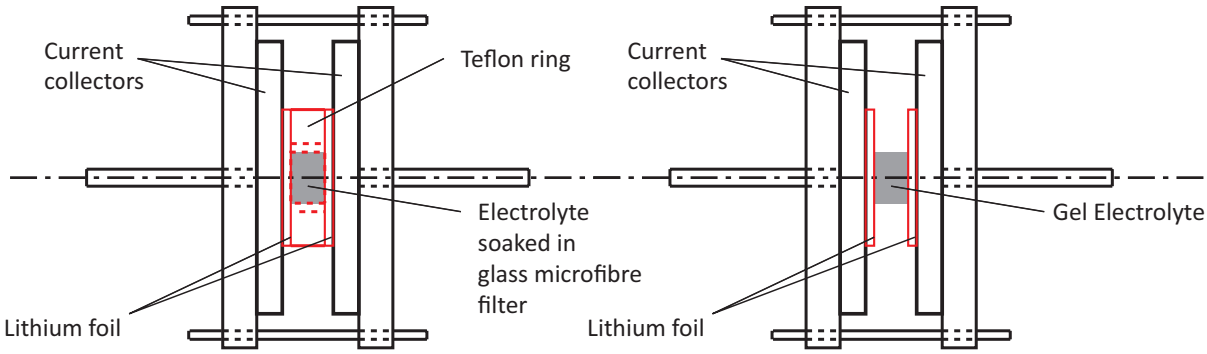

Figure 2.3: *Experimental setup of a galvanostatic polarization experiment. On the left for a liquid electrolyte and on the right for a gel electrolyte*

In order to get good fits between the simulated and experimental galvanostatic polarization experiments, care had to be taken in the choices of cell length and current density. A too long cell will have the consequence of too long experiments and a short cell will make it difficult to control the length itself. In the end 500 µm was found to be a good compromise for the liquid electrolyte. The thicknesses of the discs in the gel experiments were also in the same magnitude. Regarding the choice of current density, a high value will create dendrites, whereas the relative error in the measurement of the potential will dominate at low current densities. The current density was therefore finally chosen so that the initial relaxation potential was below 50 mV and above 5 mV.

2.5 Diffusion Experiments

In the salt and solvent diffusion experiments the circular discs of the gel were immersed in a liquid electrolyte containing $LiPF_6$ (Strem Chemicals, max 20 ppm water) dissolved in an ethylene carbonate and propylene carbonate mixture (EC:PC, 60:40, Merck, Battery Grade). The solvent and the salt were allowed to diffuse between the liquid electrolyte and the gel for a predetermined time. After the elapsed time, the weight increase or decrease of the gel was measured. The thickness and area of the gel was measured before and after the experiment, to measure the degree of swelling of the gel.

Chapter 3

Macroscopic Modelling of the Mass Transport in Electrolytes

Macroscopic modelling of the mass transport involves describing the interactions between the species in the electrolyte. In this thesis, this is done with the Maxwell-Stefan equation, which can be derived from irreversible thermodynamics (39, 40). The equation was first developed for ideal gases, but has been proven to be valid for non-ideal liquids and polymers as well (41). The equations in this section are only described briefly, but their derivation can be found in the papers. They are derived for the two types of electrolytes that is found in this thesis, (1) a liquid electrolyte where a $LiPF_6$ salt is dissolved in a mixture of EC and EMC and (2) a gel electrolyte where the same salt is dissolved in a EC-PC mixture and a P(VdF-HFP) copolymer. Four types of models that were based on these equations were implemented in COMSOL Multiphysics. Two of them describe the galvanostatic polarization experiment for the two electrolytes. The third one describe the diffusion experiments for the gel electrolyte and the final one describe the performance of a lithium-ion battery cell during a hybrid pulse power characterization (HPPC) test. In order to be consistent with the notation used in this thesis, some symbols, superscripts and subscripts can be different from the ones used in the papers.

3.1 Maxwell-Stefan Equation for Electrolytes

According to the Maxwell-Stefan equation, the driving force for the transport of one specie, F_i, is equal to the sum of the friction forces acting on that specie (eq. 3.1).

$$F_i = \sum_j \frac{RTc_i c_j}{c_{tot} d_{ij}} \left(v_j - v_i \right) \tag{3.1}$$

d_{ij}, in eq. 3.1, is the Maxwell-Stefan diffusivity for the interaction between the two species *i* and *j*. It is defined in such a way that the diffusivity that describes the interaction between species *i* and *j* is equal to the diffusivity for the interaction between *j* and *i*, i.e. $d_{ij}=d_{ji}$.

One or several driving forces can give rise to a movement of a species, for example a potential, concentration or pressure difference. As can be seen in table 3.1, a driving force of 100 J mol^{-1} is equal to a potential difference of 1 mV. A typical value of a potential drop over only the separator in a lithium-ion battery cell is at least 1 mV. The same driving force is equal to a salt concentration difference of 0.02 mol/dm^3 for a 1 mol/dm^3 electrolyte, which is common to see in lithium-ion cells. There must be a substantial pressure difference for the pressure force to be important. At least 1.3 MPa is necessary to achieve the same driving force, which is not observed in lithium-ion battery cells. Only the chemical potential gradient and the electric force are therefore included as driving forces in the Maxwell-Stefan equation.

Table 3.1: *Comparison between different driving forces. (42) The calculations are based on a 1 mol/dm^3 $LiPF_6$ (EC:EMC) electrolyte*

	Value	=	Driving force / J mol^{-1}
Electric	1 mV	=	100
Chemical potential gradient	0.02 mol/dm^3	=	100
Pressure difference	1.3 MPa	=	100

There are several possible definitions of the electric potential that can be inserted in the driving force term. Here, the electrostatic potential is added to the chemical potential to yield an electrochemical potential (8). The electrochemical potential of the lithium ion is measurable with a lithium reference electrode and is therefore directly related to the potential that is measured in the experiments. Here, this measurable potential is denoted as the quasi-electrostatic potential Φ. The expressions for the driving forces for the ions in a liquid and a gel electrolyte are seen in table 3.2.

Table 3.2: *Expressions for the driving forces for the lithium ion and hexafluorophosphate ion in a gel and liquid electrolyte*

Species / Type of Electrolyte	Lithium ion	Hexafluorophosphate ion
Liquid	$c_S F\frac{\partial \Phi}{\partial x}$	$2RT\left(1+\frac{\partial \ln f_{\pm}}{\partial \ln c_S}\right)\frac{\partial c_S}{\partial x}-c_S F\frac{\partial \Phi}{\partial x}$
Gel	$c_S F\frac{\partial \Phi}{\partial x}$	$2RT\left(1+\frac{\partial \ln f_{\pm}}{\partial \ln c_S}\right)\frac{\partial c_S}{\partial x}+2RT\frac{c_S}{c_L}\frac{\partial \ln f_{\pm}}{\partial \ln c_L}\frac{\partial c_L}{\partial x}-c_S F\frac{\partial \Phi}{\partial x}$

For a liquid electrolyte, the driving force of the hexafluorophosphate ion is dependent on the thermodynamic enhancement factor of the salt. Its value is usually one for diluted electrolytes. However, it increases at higher salt concentrations. For a gel electrolyte, two enhancement factors can be found in the expression of the driving forces, since the activity coefficient, $f_{\pm}$, is dependent on the solvent concentration as well.

An expression for the driving force of the solvent in a gel electrolyte is also needed and it is given in eq. 3.2.

$$F_L = RT\frac{c_L}{c_S}\frac{\partial \ln f_L}{\partial \ln c_S}\frac{\partial c_S}{\partial x} + RT\left(1+\frac{\partial \ln f_L}{\partial \ln c_L}\right)\frac{\partial c_L}{\partial x} \tag{3.2}$$

On the R.H.S of eq. 3.1, the interactions between the species are described by the Maxwell-Stefan diffusivities, d_{ij}. There exists one diffusivity for each interaction. For example, there is one diffusivity describing the interaction between the ions and two for the interactions between the ions and the solvent, for an electrolyte that contains a salt (two ions) dissolved in a solvent. A higher value of the diffusivity means less interaction between the species. For an ideal gas, the diffusivities are constants and only dependent on the two species they describe the interaction between. However, for a nonideal fluid the diffusivities are dependent on the composition of the fluid (8).

For an electrolyte with *n* species, it is only possible to get *(n-1)* independent equations from the Maxwell-Stefan equation. To get expressions for all the species' velocities, v_i, an additional equation must be introduced. If the partial molar volumes of the species in the system, V_m^i, are independent of the composition, the additional equation can be a volume balance (eq. 3.3). The equation can be solved by knowing the fluxes at the boundaries.

$$\sum_j V_m^j \frac{\partial N_j}{\partial x} = 0 \tag{3.3}$$

The fluxes of all the species in the equation can then be calculated by inverting the Maxwell-Stefan equation. To ensure electroneutrality, the concentrations of the lithium ions and hexafluorophosphate ions are set to the same value. The last step in the derivation, is to introduce the current density, *i*, which is done by expressing it in terms of the fluxes of the ions (eq. 3.4).

$$i = F\left(N_+ - N_-\right) \tag{3.4}$$

There are two types of equations that come out of the Maxwell-Stefan equation for electrolytes. First, there are expressions of the fluxes as a function of the driving forces. These can be inserted in a material balance from which the concentration profiles can be

calculated. The second one is an equation that describes the potential gradients as a function of the current density and the concentration gradients and it is needed for calculating the potential drop over the electrolyte.

3.2 Transport Properties for $LiPF_6$ dissolved in EC and EMC

For the liquid electrolyte that contains $LiPF_6$ dissolved in a solvent mixture of EC and EMC, the material balance is expressed as eq. 3.5. The solvent mixture is treated as one specie in the model, since the properties of the two solvents are similar (22).

$$\frac{\partial c_S}{\partial t} = \frac{\partial}{\partial x}\left[D_S \frac{\partial c_S}{\partial x} + (1 - t_+)\frac{i}{F} \right] \tag{3.5}$$

The variation of the potential in the electrolyte is described by eq. 3.6. The potential increases with higher current densities and higher concentration gradients. The equation describe how the potential varies in the electrolyte when it is measured with a lithium reference electrode.

$$\frac{\partial \Phi}{\partial x} = -\frac{i}{\kappa} + \eta_S \frac{\partial c_S}{\partial x} \tag{3.6}$$

Table 3.3: *Different groups of apparent transport properties for liquid electrolytes*

Transport properties	Expressions
D_S	$\frac{2d_{+L}d_{-L}}{d_{+L}+d_{-L}}\left(1+\frac{\partial \ln f_{\pm}}{\partial \ln c_S}\right)\frac{c_{tot}}{c_L}\left(1-c_S V_m^S\right)$
t_+	$1-\left(1-c_S V_m^S\right)\cdot\frac{d_{-L}}{d_{+L}+d_{-L}}$
κ	$\left[\frac{RT}{c_{tot}F^2}\left(\frac{1}{d_{+-}}+\frac{c_L\left(d_{+L}+d_{-L}\right)}{c_S}\right)\right]^{-1}$
η_S	$\frac{2RT}{c_S}\left(1+\frac{\partial \ln f_{\pm}}{\partial \ln c_S}\right)\left(\frac{d_{-L}}{d_{+L}+d_{-L}}\right)$
$\widetilde{D}_S$	$\frac{2d_{+L}d_{-L}}{d_{+L}+d_{-L}}$
t_+^L	$\frac{d_{+L}}{d_{+L}+d_{-L}}$

In the above equations, a set of four coefficients can be found. The upper part of table 3.3 shows their dependence on the composition, Maxwell-Stefan diffusivities,

thermodynamic enhancement factors and molar volumes. The coefficients are apparent transport properties, since they describe all the processes that were taken into account in the derivation of the equations. For example, the lithium ion transport number includes a factor that takes into account a movement in the solvent to compensate for volume changes when the salt concentration varies. Sometimes, it is useful to define transport properties that are only dependent on the Maxwell-Stefan diffusivities. Two transport properties that are defined in such way are listed in the two last rows of the table. They are only dependent on the interactions between the species.

3.3 Transport Properties for $LiPF_6$ dissolved in EC, PC and P(VdF-HFP)

For a gel electrolyte that contains $LiPF_6$ dissolved in a mixture of EC, PC and P(VdF-HFP) the material balance for the salt is expressed as eq. 3.7.

$$\frac{\partial c_S}{\partial t} = \frac{\partial}{\partial x}\left[D_{SS} \frac{\partial c_S}{\partial x} + D_{SL} \frac{\partial c_L}{\partial x} + (1 - t_+) \frac{i}{F} \right] \tag{3.7}$$

The solvent mixture is treated as one specie, here too. The material balance for the solvent mixture is expressed as eq. 3.8.

$$\frac{\partial c_L}{\partial t} = \frac{\partial}{\partial x}\left[D_{LS} \frac{\partial c_S}{\partial x} + D_{LL} \frac{\partial c_L}{\partial x} - t_L \frac{i}{F} \right] \tag{3.8}$$

The potential is described by eq. 3.9. The potential increases with higher current densities, higher salt concentrations gradients and higher solvent concentration gradients.

$$\frac{\partial \Phi}{\partial x} = -\frac{i}{\kappa} + \eta_S \frac{\partial c_S}{\partial x} + \eta_L \frac{\partial c_L}{\partial x} \tag{3.9}$$

The set of transport properties that describes the transport in a gel electrolyte contains more independent parameters and their dependence on the Maxwell-Stefan diffusivities is more complicated than in the liquid electrolyte model. They are presented in table 3.4 together with a specification of which parameters they are dependent on. The expressions for each transport property are presented in paper III.

Table 3.4: *Different groups of apparent transport properties for a gel electrolyte*

Transport properties	Functions of…
$D_{SS}, D_{SL}, D_{LS}, D_{LL}$	Composition, Maxwell-Stefan (M-S) diffusivities, thermodynamic enhancement factors and molar volumes
t_+, t_L	M-S diffusivities and molar volumes
κ	Composition and M-S diffusivities
η_S, η_L	Composition, M-S diffusivities, thermodynamic enhancement factors

3.4 Electrolyte Mass Transport in Separators and Porous Electrodes

The mass transport in an electrolyte that is soaked into a separator or a porous electrolyte worsens, due to two factors. First, the effective concentration is decreased due to the porosity, ε.

$$c_i^{eff} = \varepsilon \cdot c_i \tag{3.10}$$

Then, the Maxwell-Stefan diffusivities are decreased due to the tortuosity, τ, and the porosity, ε (eq. 3.11). The tortuosity can then be expressed in terms of the porosity as in eq. 3.12, where γ is a scaling parameter and β is the Bruggeman coefficient.

$$d_{ij}^{eff} = \frac{\varepsilon}{\tau} d_{ij} \tag{3.11}$$

$$\tau = \gamma \cdot \varepsilon^{1-\beta} \tag{3.12}$$

Some typical values of the Bruggeman coefficient, the porosity and the scaling parameter for several separators and electrodes are found in table 3.5. In general the conductivity is worsened by a factor of 5-40 when the electrolyte is soaked into the porous material listed in the table.

Table 3.5: *Values of the Bruggeman coefficient, the porosity and the scaling parameter for different separators and electrodes.*

	γ	ε	β	Ref.
Celgard 2325	1	0.4	2.25	Paper II
Celgard 2400	1	0.37	2.8	(43)
Graphite electrode	1	0.31	2.854	(44)
NCA electrode	1	0.29	2.928	(45)
$LiFePO_4$ electrode	1.8	0.3-0.5	1.53	(46)

3.5 Macroscopic Modelling of Characterization Experiments

Models of the galvanostatic polarization experiment and the diffusion experiment were implemented and solved in COMSOL Multiphysics, so that they could be optimized to experimental data with the transport properties as optimization parameters. The optimization procedure is explained further in the next chapter, whereas the models are explained here.

The galvanostatic polarization experiment was modelled for a one-dimensional geometry with the boundaries at x=0 and *L*. During both the polarization and the relaxation parts of the experiment, the flux of the lithium ions can be expressed as eq. 3.13 at the boundaries, while the flux of the other species is equal to zero.

$$N_+ = \frac{i}{F} \qquad x = 0 \,\&\, L \tag{3.13}$$

The current density is given by eq. 3.14, where I_{pol} is the polarization current, A is the area of the electrodes and t_{pol} is the polarization time.

$$i = \begin{cases} I_{pol} / A & t < t_{pol} \\ 0 & t \geq t_{pol} \end{cases} \tag{3.14}$$

The concentration profiles are calculated by solving eq. 3.5 or 3.7. The diffusion potential is then calculated from the concentration profiles by integrating eq. 3.6 or 3.9 from x=0 to x=*L*.

For the diffusion experiments, the model is formulated for a 2D-axisymmetrical geometry (eqs 3.15 and 3.16).

$$\frac{\partial c_S}{\partial t} = \frac{1}{r}\frac{\partial}{\partial r}\left(rD_{SS}\frac{\partial c_S}{\partial r} + rD_{SL}\frac{\partial c_L}{\partial r} \right) + \frac{\partial}{\partial z}\left(D_{SS}\frac{\partial c_S}{\partial z} + D_{SL}\frac{\partial c_L}{\partial z} \right) \tag{3.15}$$

$$\frac{\partial c_L}{\partial t} = \frac{1}{r}\frac{\partial}{\partial r}\left(rD_{LS}\frac{\partial c_S}{\partial r} + rD_{LL}\frac{\partial c_L}{\partial r}\right) + \frac{\partial}{\partial z}\left(D_{LS}\frac{\partial c_S}{\partial z} + D_{LL}\frac{\partial c_L}{\partial z}\right) \tag{3.16}$$

The gel was shaped as a disc and surrounded by a liquid electrolyte. Mass transport occurred between the liquid and the gel, but it is assumed that the mass transport limitations occurred in the gel only. The boundary conditions are expressed as eq. 3.17, where the concentrations of the liquid electrolyte are c_S^{liquid} and c_L^{liquid}.

$$\left.\begin{aligned} c_S &= c_S^{liquid} \\ c_L &= c_L^{liquid} \end{aligned}\right\} r = \pm R_d \quad z = \pm\frac{L}{2} \tag{3.17}$$

The total mass of the gel after the diffusion experiment is calculated by integrating the concentrations expressed as g/m^3 over the volume of the disc.

3.6 Macroscopic Modelling of a Li-Ion Cell during HPPC-tests

The performance of a lithium-ion cell was simulated during a HPPC test, so that mass transport limitations in the liquid electrolyte could be studied during conditions similar to those in a hybrid electrical vehicle. A schematic figure of the processes that occur during charging and discharging of a lithium-ion cell is seen in figure 3.1.

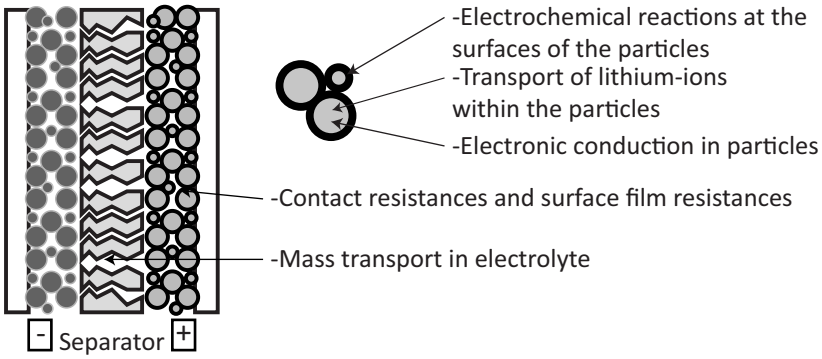

Figure 3.1: *Schematic figure of the processes in a lithium-ion cell*

During discharge, lithium ions are transported from the active material in the negative electrode to the active material in the positive electrode and electrons are transported in an outer circuit in the opposite direction. There are several processes that occur in the cell and each of them is described by their own equations. All equations that were used in the model are presented in paper II. Here, only the equations for the mass transport in the electrolyte are presented.

When the lithium ions are transported between the electrodes, the salt concentration profile can be described by eq. 3.18.

$$\varepsilon \frac{\partial c_S}{\partial t} = \frac{\partial}{\partial x}\left[\frac{\varepsilon^\beta}{\gamma} D_S \frac{\partial c_S}{\partial x} + \left(1 - t_+\right) \frac{j_P}{F} \right] \tag{3.18}$$

j_P is the current density in the pores of the electrodes and separator. It will vary within the porous electrodes according to eq. 3.19 due to intercalation or de-intercalation of lithium ions at the surfaces. j_{loc} is the local reaction rate and a is the specific surface of the electrode.

$$\frac{\partial j_P}{\partial x} = a j_{loc} \tag{3.19}$$

The potential distribution in the electrolyte, Φ_P, is calculated from eq. 3.20.

$$j_P = \kappa \cdot \frac{\varepsilon^\beta}{\gamma} \cdot \left(-\frac{\partial \Phi_P}{\partial x} + \eta_S \frac{\partial c_S}{\partial x} \right) \tag{3.20}$$

The model was used to simulate two HPPC tests that were defined by EUCAR (47) and ISO. In the tests, the current varied according to figure 3.2a and b. The ISO-energy cycle covers a SOC span (ΔSOC) of 20 %, which indicates that it strains the cell more than the EUCAR cycle with a ΔSOC of 5 %. For the simulated battery, 1 C was equal to 9.92 A m^{-2}.

A strategy for analysing the data from the battery model was set up. The strategy is based on studying and quantifying the different processes in the cell in terms of their influence on the polarization. In a battery cell with planar electrodes, the polarization can easily be split up into parts that are associated with a process. In contrast, for porous electrodes the electrochemical reaction is spread out in the electrode so that the total polarization is minimized. The electrochemical reaction occurs therefore at different conditions in the electrode and, thus, the polarization that is associated with, e.g., the activation of the electrochemical reaction varies. Yet, an average value of the polarization that each process causes can be calculated by integrating the product of the local polarization and the current density that caused it and normalize it with the total current density. The expressions that were used in these calculations are listed in table 3.6.

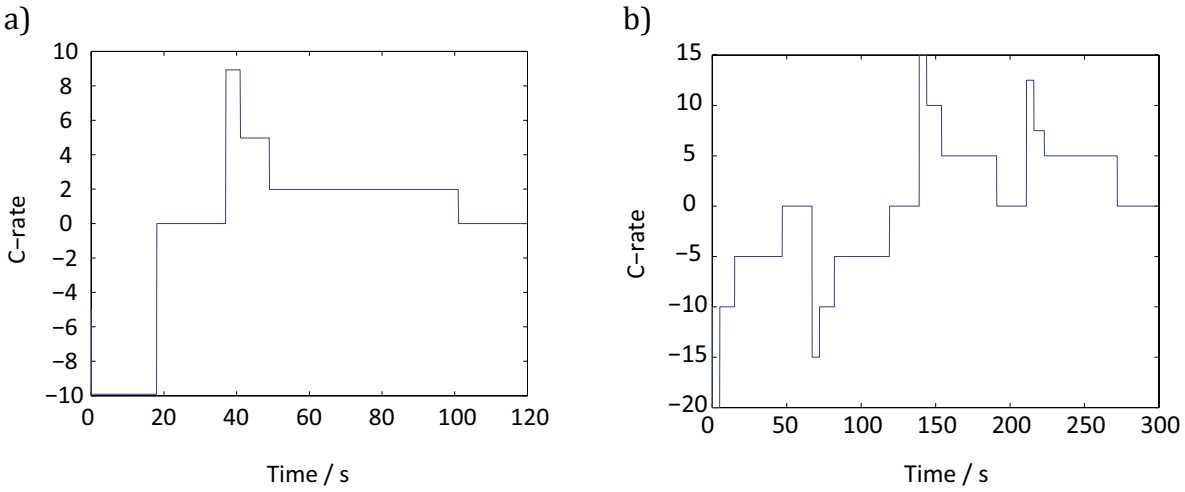

Figure 3.2: *The C-rate as function of time during a HPPC test according to a) EUCAR and b) ISO*

Table 3.6: *Expressions for calculations of the polarizations due to each process*

Process	*Expression*
Diffusion polarization electrolyte	$-\frac{1}{j_{tot}}\int j_P \eta_S \frac{\partial c_S}{\partial x} dx$
Diffusion polarization solid phase	$\frac{1}{j_{tot}}\int a j_{loc}\left(E_{surf} - E_{ave}\right) dx$
Ohmic potential drop electrolyte	$\frac{1}{j_{tot}}\int \frac{\gamma\left(j_P\right)^2}{\varepsilon^\beta \kappa} dx$
Ohmic potential drop solid phase	$\frac{1}{j_{tot}}\int \frac{\left(j_M\right)^2}{\sigma_{eff}} dx$
Activation overpotential	$\frac{1}{j_{tot}}\int a j_{loc}\left(\Phi_M - \Phi_P - E_{surf}\right) dx$
Contact resistance	$j_{appl} R_{contact}$

E_{surf} is the equilibrium potential of the electrode immediately after the current is switched off and E_{ave} is the equilibrium potential of the electrode at an infinite time after the current is switched off. j_M and Φ_M are the current density and potential in the conducting material of the electrodes. An inherent property of the model is that the sum of the polarizations listed in the table is equal to the total polarization of the cell. Calculating the averaged value of the polarization associated with the processes displayed in figure 3.1 allows us to compare them with each other and to determine for which conditions the mass transport in the electrolyte is responsible for increased polarization in the cell. To analyze the contribution to the polarization over the whole HPPC cycle, a cycle-averaged polarization was defined according to eq. 3.21, where $\eta_{ave,j}$ is any of the polarizations listed in the table above. The cycle-averaged polarization is

calculated as a rate of energy loss due to the process in question, integrated over time and normalized with the total amount of charged passed during the cycle.

$$\eta_{ave,i}^{cycle} = \frac{1}{\int_0^{t_{cycle}} |j_{tot}| dt} \int_0^{t_{cycle}} \eta_{ave,i} j_{tot} dt \tag{3.21}$$

Chapter 4

Extraction of Transport Properties from Characterization Experiments

The transport properties were extracted from the response of the characterization experiments in three steps. First, the conductivity was calculated from the conductivity measurements. Then the relationships between a change in the composition and a change of the potential of the electrolyte were extracted from concentration cell data. Lastly, the diffusion coefficients and the transport numbers were obtained in an optimization scheme, where models of some characterization experiments were optimized to experimental data.

4.1 Conductivity measurements

Conductivity measurements are quick experiments that can be easily performed for a variety of electrolytes. The conductivity of the liquid electrolyte was measured with a standard conductometer where the value of the conductivity was given directly on a display, while the conductivity of the gel electrolyte was measured with electrochemical impedance spectroscopy. The impedance spectra were plotted in a Nyquist plot and the intercept on the real axis was interpreted as the electrolyte resistance, $R_{electrolyte}$. The conductivity was then calculated from eq. 4.1, where A and L are the area and thickness of the gel.

$$\kappa = \frac{L}{A \cdot R_{electrolyte}} \tag{4.1}$$

4.2 Concentration Cells

The concentration cell experiments were performed to obtain the relation between a concentration profile and a potential profile in the electrolyte. This is equivalent to

obtaining the potential of an electrolyte as a function of its composition. Experiments were performed where both the concentration difference between the two samples and the average concentration of them were varied. The data was then fitted to a polynomial in MATLAB. The polynomials that were found to describe the experimental data best are shown in eq. 4.2 for the liquid electrolyte and eq. 4.3 for the gel electrolyte, where the indices 1 and 2 stand for the two electrolytes in the experiment. The fits of the polynomials to the experimental data were good.

$$\Delta\Phi\big|_{i=0} = \frac{2RT}{F}\left(\alpha_1\left(c_{S,2}^2 - c_{S,1}^2\right) + \alpha_2\left(c_{S,2} - c_{S,1}\right) + \alpha_3 \ln\left(\frac{c_{S,2}}{c_{S,1}}\right)\right) \tag{4.2}$$

$$\Delta\Phi\big|_{i=0} = \alpha_1\left(c_{S,2} - c_{S,1}\right) + \alpha_2 \ln\left(\frac{c_{S,2}}{c_{S,1}}\right) + \alpha_3\left(c_{L,2} - c_{L,1}\right) + \alpha_4 \ln\left(\frac{c_{L,2}}{c_{L,1}}\right) \tag{4.3}$$

The parameter η_S, which is defined in eq. 3.6 (liquid electrolyte) and 3.9 (gel electrolyte), were then calculated by computing the derivate of eq. 4.2 and 4.3 with respect to the salt concentration. The parameter η_L was calculated by computing the derivate of eq. 4.3 with respect to the solvent concentration.

4.3 Extraction of Diffusion Coefficients and Transport Numbers

Values of the diffusion coefficients and the transport numbers were extracted from the characterization experiments by fitting models of the experiments to experimental data (c.f. chapter 3.5). The models were solved for different values of the transport properties in COMSOL Multiphysics (figure 4.1), while the program "lsqnonlin" in the MATLAB optimization toolbox was employed as the optimization algorithm.

The program tried to minimize an objective function, which compared the experimental and simulated data. The loop in figure 4.1 continued until the minimum value of the objective function was found. For the liquid electrolyte, the objective function was defined as eq. 4.4.

$$\chi = \sum_i \left(\Phi^{\text{model}}\left(t_i\right) - \Phi^{\exp}\left(t_i\right)\right)^2 \tag{4.4}$$

For the gel electrolyte, the objective function was defined as eq. 4.5, where the value of the weight factor W_1 was chosen so that the two types of experiments had equal importance. The values in the denominator are the estimated errors in each experiment.

$$\chi = W_1 \cdot \sum_i \left(\frac{\Phi^{\text{model}}(t_i) - \Phi^{\text{exp}}(t_i)}{\Phi^{\text{exp}}(t_i) + 0.005} \right)^2 + \sum_i \left(\frac{\Delta m^{\text{model}}(t_i) - \Delta m^{\text{exp}}(t_i)}{\Delta m^{\text{exp}}(t_i) + 0.001} \right)^2 \tag{4.5}$$

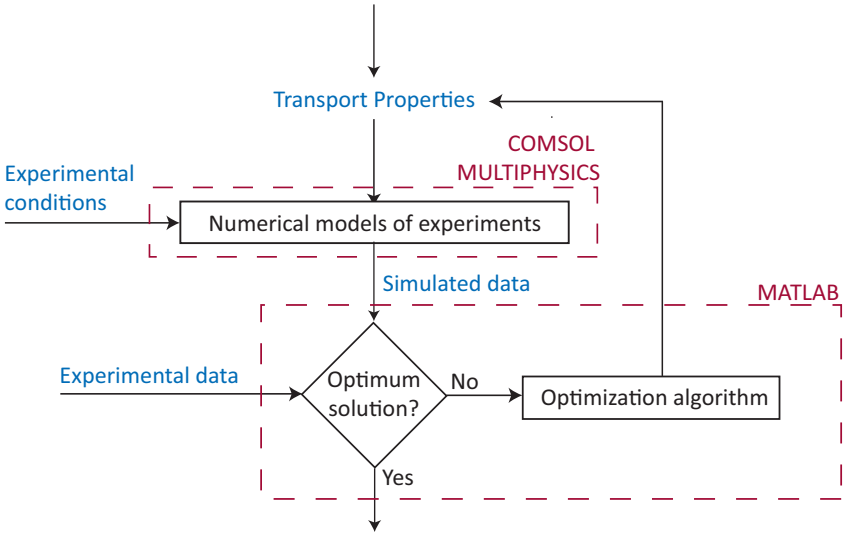

Figure 4.1: *Optimization strategy for the estimation of the diffusion coefficients and the transport numbers*

A mathematical analysis of the characterization experiments of the gel electrolyte was done before the actual characterization, to assure that the four diffusion coefficients and two transport numbers could be extracted from the experiments in an effective way. The characterization method used for the gel is based on the one developed for liquid electrolytes. An analysis of that method will therefore be presented first, even if the method is fairly well established by now.

A schematic figure of the characterization method for the liquid electrolyte is seen in figure 4.2. The transport properties that are obtained in the characterization are defined in chapter 3. The characterization method was initially developed for polymer electrolytes (one salt dissolved in one polymer) (25), but it has been successfully used for the liquid electrolytes as well (9). D_S is obtained from the galvanostatic polarization experiments, while t_+ is obtained by combining the experimental response of the galvanostatic polarization experiment with data from the concentration cells. Ψ, which is used when calculating t_+, is included in the figure although it is not an apparent transport property. It is defined in eq. 4.6 and its importance will be discussed later.

$$\Psi = \eta_S \frac{(1 - t_+)}{D_S} \tag{4.6}$$

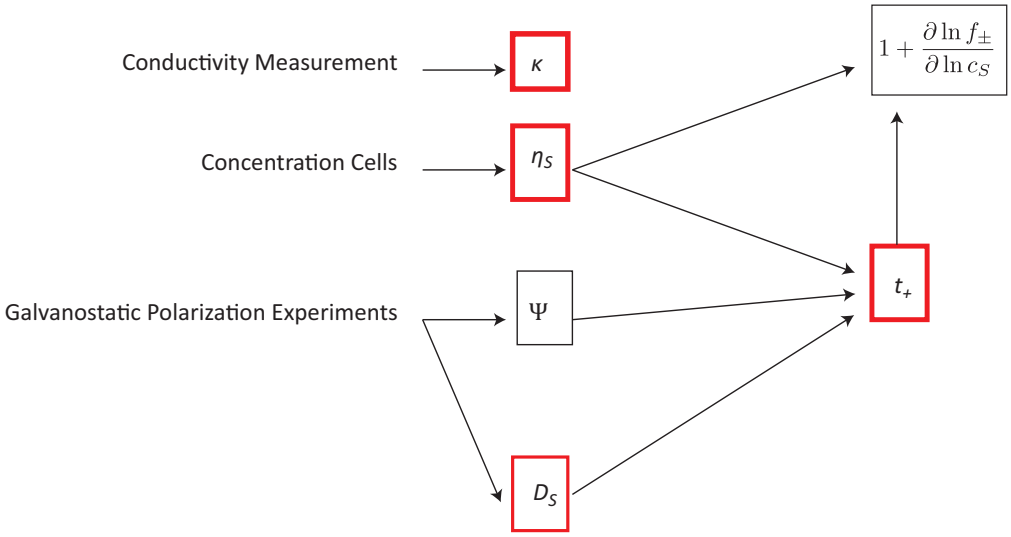

Figure 4.2: *Schematic figure of the characterization method for liquid electrolytes. The highlighted squares are apparent transport properties*

The parameter η_S is implemented in the mass transport model as a polynomial and the model is then fitted to the response of the galvanostatic polarization experiments to obtain both D_S and t_+.

In the galvanostatic polarization experiment, the electrolyte is polarized for a pre-determined time. During the polarization, a concentration profile is built up, which causes the diffusion potential to increase. If the electrolyte is polarized during a long period with a large current, the diffusion potential will consequently be large as well. For a very long period of polarization, it will reach its steady-state value. The concentration profile and the diffusion potential start to relax when the current is switched off. The shape of the relaxation is dependent on how fast the salt is diffusing and thus the salt diffusion coefficient, while the initial diffusion potential (Ψ in figure 4.2) is dependent on the magnitude of the concentration difference that has been formed during the polarization and is thus dependent on both the lithium ion transport number and the salt diffusion coefficient. Eq. 4.7 describes the diffusion potential during the relaxation. It is derived in paper III with the assumption that the apparent transport properties are constant in the relatively narrow concentration range of the experiment.

$$\Delta\Phi_{rel} = \frac{8}{\pi^2}\cdot\frac{i\cdot L}{F}\sum_{m=1}^{\infty}\left[\frac{\Psi}{(2m-1)^2}\left(\exp\left(-\frac{(2m-1)^2\pi^2 D_S\left(t-t_{pol}\right)}{L^2}\right)-\exp\left(-\frac{(2m-1)^2\pi^2 D_S t}{L^2}\right)\right)\right] \tag{4.7}$$

As expected, two effective parameters can be obtained from the equation, Ψ and D_S. However, eq. 4.7 can be simplified at certain conditions. For example, Hafezi *et al.* (32) have used a simplified version of this equation to obtain a parameter, which is dependent on D_S, t_+ and η_S. It is derived using the assumption that the diffusion is semi

infinite and they found that the relaxation of the diffusion potential is proportional to a dimensionless time (eq. 4.8).

$$\Delta\Phi = 4\eta_S L\frac{(1-t_+)i}{D_S F}\sqrt{\frac{D_S t_{pol}}{L^2\pi}}\underbrace{\left(\frac{\sqrt{t_{pol}}}{\sqrt{t}+\sqrt{t-t_{pol}}}\right)}_{\tau} \tag{4.8}$$

Only one parameter can be extracted from eq. 4.8, that is the slope of a $\Delta\Phi$ versus τ plot. This has the consequence that it is not possible to obtain both the transport number and the salt diffusion coefficient if the conditions in the cell are semi-infinite. The parameter that decides whether the conditions are semi-infinite or not is the product $D_S t_{pol}/L^2$. In figure 4.3, it can be seen for which $D_S t_{pol}/L^2$ values that eq. 4.8 is valid.

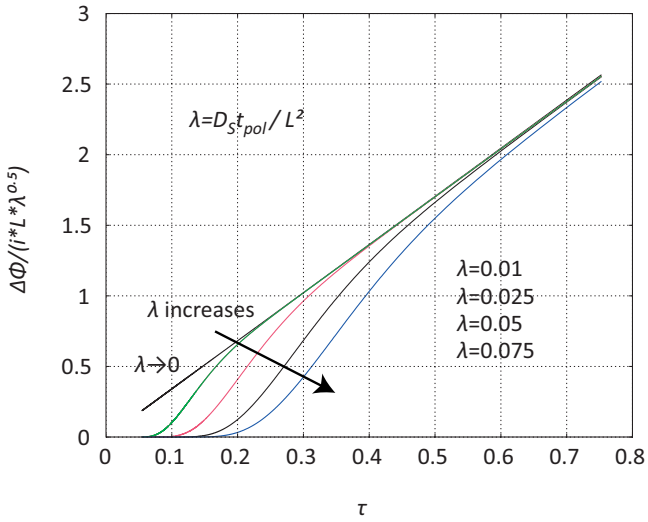

Figure 4.3: *Simulated values of the diffusion potential plotted as a function of the dimensionless time for different $D_S t_{pol}/L^2$ values. The data was calculated from eqs 3.5-3.6 and eqs 3.13-3.14 with COMSOL Multiphysics. The dimensionless time was defined by Hafezi et al. (32)*

As the value of $D_S t_{pol}/L^2$ increases, the linearity with the dimensionless time disappears. For $D_S t_{pol}/L^2 > 0.025$ it is hard to define any straight slope and D_S and t_+ can therefore be independently obtained from the experimental data at those conditions.

As seen in eq. 4.7, the diffusion potential can be made independent of the thickness of the cell, the current density and the polarization time by plotting $\Delta\Phi/(i*L)$ versus t_{pol}/L^2 and $(t-t_{pol})/L^2$. In figure 4.4, simulated data of the relaxation of the diffusion potential in an electrolyte is plotted in such way. The shape of the surface is only dependent on the transport properties and the composition of the electrolyte. The aim of the optimization is to catch the shape of this surface in the values of t_+ and D_S.

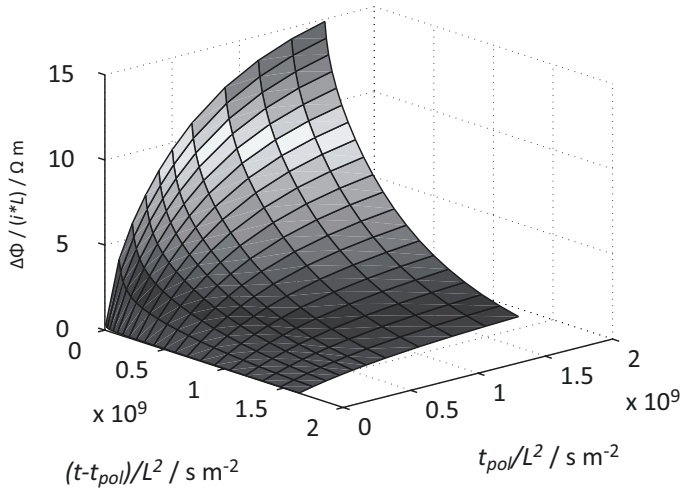

Figure 4.4: *The relaxation of the diffusion potential for different t_{pol}/L^2 values.*

Figure 4.5 shows examples of experimental results from paper I, together with modelled relaxation profiles using the obtained optimized parameters. The agreement between the optimised profile and the experimental one is good. All galvanostatic polarization experiments that were used in the characterization in paper I had a $D_S t_{pol}/L^2$ value higher than 0.04, to assure finite conditions.

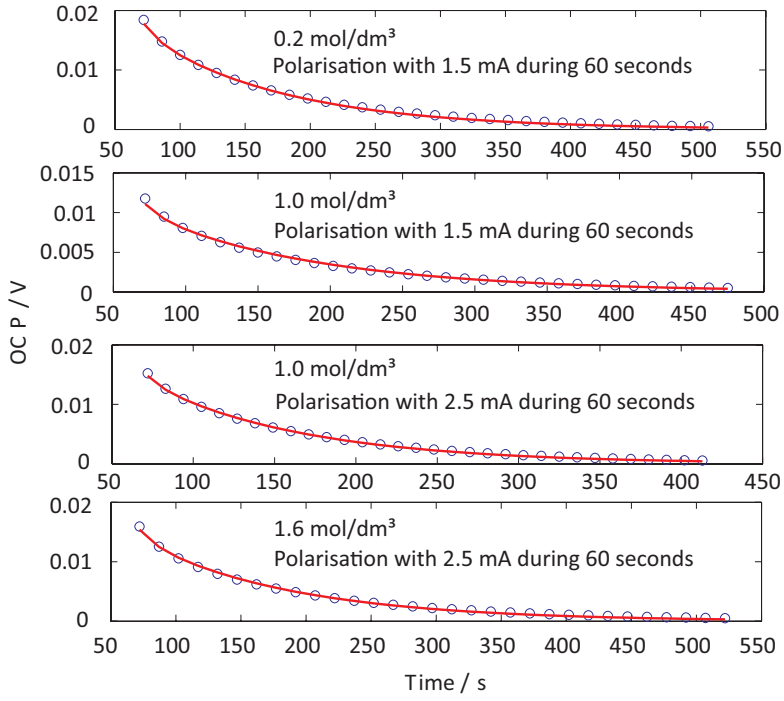

Figure 4.5: *Four typical relaxations of the open circuit potential after a galvanostatic polarization for 0.2 mol/dm³, 1.0 mol/dm³ and 1.6 mol/dm³ $LiPF_6$ EC-EMC. Experimental results (o) and simulated results (-)*

For the characterization method used for gel electrolytes, the apparent transport properties are obtained from the experiments according to the scheme in figure 4.6.

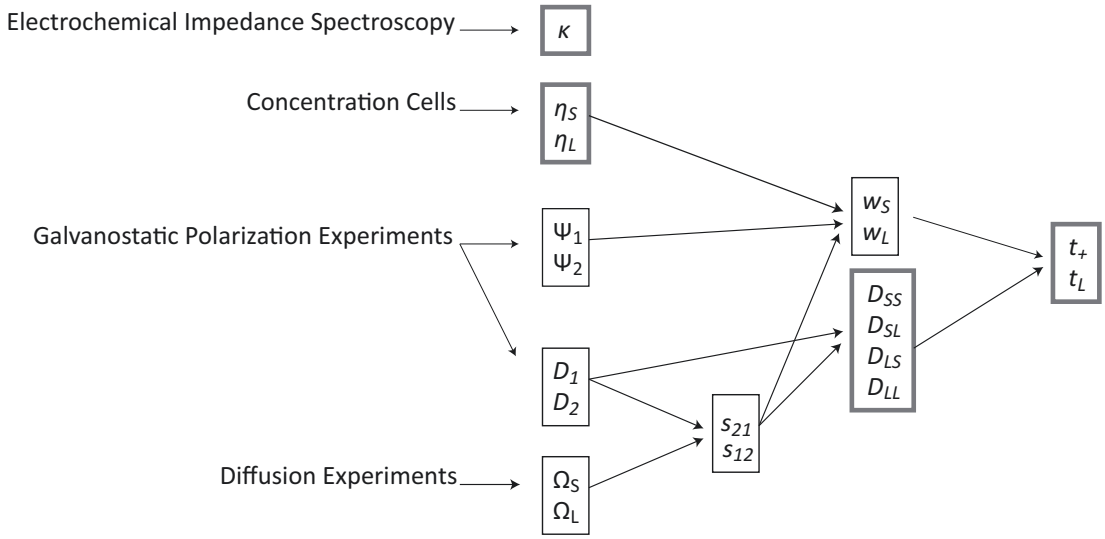

Figure 4.6: *Schematic figure of the characterization method for gel electrolytes. The highlighted squares are apparent transport properties*

The scheme is more complicated than the one for liquid electrolytes, since the number of transport properties has increased. The highlighted squares are apparent transport properties (c.f. table 3.4) while the parameters to the left describe each experiment. The parameters s_{21}, s_{12} ,w_S and w_L are shown in the figure to illustrate the relationships between the experiments and the apparent transport properties. They are all defined in table 4.1 and they will be discussed later. The transport numbers and the diffusion coefficients are obtained by fitting models of the diffusion experiment and the galvanostatic polarization experiment to experimental data. η_S and η_L are implemented in the models as polynomials of the composition.

In paper III, an expression for the relaxation of the diffusion potential during the galvanostatic polarization experiment is derived and it is presented in eq. 4.9. The expression is derived with the assumption that transport properties are constant. There are four effective parameters that can be identified in the expression. Their dependence on the transport properties is shown in table 4.1.

$$\Delta\Phi_{rel} = \frac{8}{\pi^2}\cdot\frac{i\cdot L}{F}\sum_{m=1}^{\infty}\left[\begin{array}{l}\dfrac{\Psi_1}{(2m-1)^2}\left(\exp\left(-\dfrac{(2m-1)^2\pi^2 D_1\left(t-t_{pol}\right)}{L^2}\right)-\exp\left(-\dfrac{(2m-1)^2\pi^2 D_1 t}{L^2}\right)\right)+\\ \dfrac{\Psi_2}{(2m-1)^2}\left(\exp\left(-\dfrac{(2m-1)^2\pi^2 D_2\left(t-t_{pol}\right)}{L^2}\right)-\exp\left(-\dfrac{(2m-1)^2\pi^2 D_2 t}{L^2}\right)\right)\end{array}\right] \quad (4.9)$$

The expression has some similarities with eq. 4.7. As a matter of fact, the relaxation of the diffusion potential in a gel electrolyte can be said to be the sum of two relaxations of the diffusion potentials in two different binary electrolytes. In the equation, D_1 and D_2 are related to the shape of the relaxation, while Ψ_1 and Ψ_2 are related to the initial value of the diffusion potential. At large t_{pol}/L^2 values, the term with the lowest D_k value will dominate and at small t_{pol}/L^2 values, the term with the highest D_k value will dominate. The equation has similar properties as eq. 4.7. If the diffusion in the gel is semi-infinite, that is $D_2 t_{pol}/L^2 < 0.025$, the sum of the exponential terms can be simplified to a linear dependence of the dimensionless time. Only one parameter can then be extracted from the experiments.

The aim of an optimization is to catch the shape of the $\Delta\Phi/(i^*L)$ versus t_{pol}/L^2 and $(t-t_{pol})/L^2$ surface in the values of transport properties. An ideal set of characterization experiments should span t_{pol}/L^2 values in a span from 0 to a value where the shape of the plot $\Delta\Phi/(i^*L)$ versus $(t-t_{pol})/L^2$ is not changing anymore.

Table 4.1: *Definitions of parameters that occur in eq. 4.9*

Parameter	Expression
Ψ_1	$\frac{(\eta_S - \eta_L s_{12})(w_S + s_{21} w_L)}{1 - s_{21} s_{12}}$
Ψ_2	$-\frac{(\eta_S s_{21} - \eta_L)(s_{12} w_S + w_L)}{1 - s_{21} s_{12}}$
D_1	$\frac{D_{LL} + D_{SS} + \sqrt{(D_{LL} - D_{SS})^2 + 4 D_{LS} D_{SL}}}{2}$
D_2	$\frac{D_{LL} + D_{SS} - \sqrt{(D_{LL} - D_{SS})^2 + 4 D_{LS} D_{SL}}}{2}$
s_{21}	$\frac{D_{LL} - D_{SS} + \sqrt{(D_{LL} - D_{SS})^2 + 4 D_{LS} D_{SL}}}{2 D_{LS}}$
s_{12}	$\frac{D_{SS} - D_{LL} - \sqrt{(D_{LL} - D_{SS})^2 + 4 D_{LS} D_{SL}}}{2 D_{SL}}$
w_S	$-\frac{D_{LL}(1 - t_+) + D_{SL} t_L}{D_{SS} D_{LL} - D_{SL} D_{LS}}$
w_L	$\frac{D_{LS}(1 - t_+) + D_{SS} t_L}{D_{SS} D_{LL} - D_{SL} D_{LS}}$

Figure 4.7 shows examples of experimental and simulated results from paper III. The profiles were simulated with the optimum set of transport properties. The agreement between the optimized profile and the experimental one is good. The experiments were performed at different t_{pol}/L^2 values, to ensure that all four parameters could be extracted. The experiment with the lowest t_{pol}/L^2 value is performed very close to semi-infinite conditions.

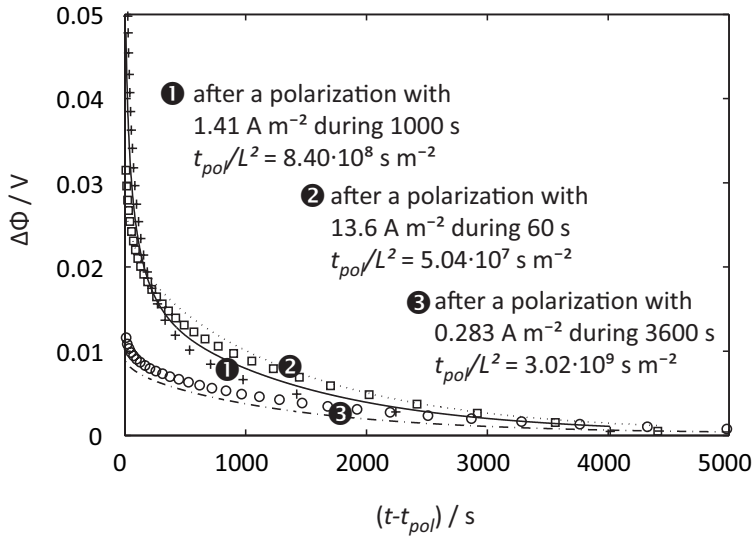

Figure 4.7: *Four typical relaxations of the open circuit potential after a galvanostatic polarization for a gel containing 45 % P(VdF-HFP), 9 % $LiPF_6$ and 46 % EC-PC.* (o,+,□) *Experimental results and (-,--,-.-) simulated results*

In the diffusion experiments, a disc of the gel is immersed in a liquid electrolyte for a predetermined time, t_c, and the solvents and the salt are allowed to be transported between the liquid electrolyte and the gel through diffusion. If the diffusion during the experiment is semi-infinite, the increase of the mass at the time, t_c, is described by eq. 4.10.

$$\Delta m_{gel} = \frac{2 \cdot A \cdot t_c^{0.5}}{\pi^{0.5}} \left(\Omega_S \left(c_S^{liquid} - c_S^0 \right) + \Omega_L \left(c_L^{liquid} - c_L^0 \right) \right) \tag{4.10}$$

Where Ω_S and Ω_L are defined as:

$$\Omega_S = \frac{M_S^w \left(D_1^{0.5} - s_{21} s_{12} D_2^{0.5} \right) - M_L^w s_{12} \left(D_1^{0.5} - D_2^{0.5} \right)}{1 - s_{21} s_{12}} \tag{4.11}$$

$$\Omega_L = \frac{M_S^w s_{21} \left(D_1^{0.5} - D_2^{0.5} \right) - M_L^w \left(s_{12} s_{21} D_1^{0.5} - D_2^{0.5} \right)}{1 - s_{21} s_{12}} \tag{4.12}$$

The two parameters Ω_S and Ω_L, can be obtained by combining several diffusion experiments where both the contact time t_c and the composition in the liquid c_S^0 and c_L^0 are varied. Examples of experimental data are seen in figure 4.8, together with simulated data with the optimum set of transport properties. The model seems to catch the increase of the mass during the experiments.

As for the galvanostatic polarization experiment, more parameters could be extracted from the experiment if it was performed at finite conditions. However in the characterization in paper IV, most experiments were performed at semi-infinite conditions, since it was experimentally difficult to perform experiments during longer time periods.

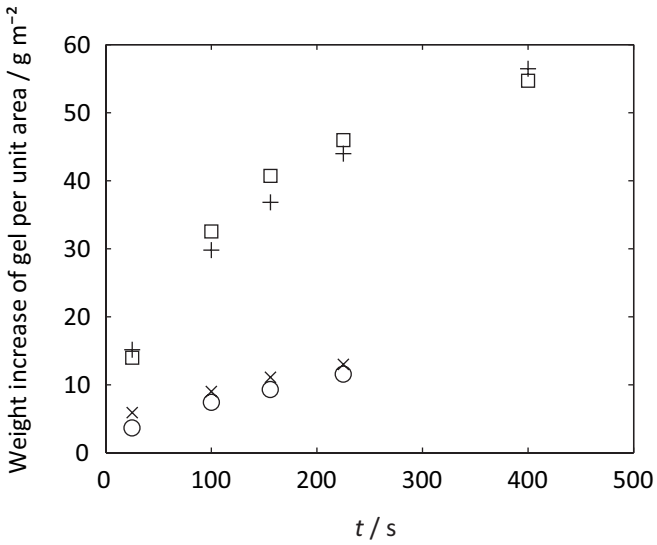

Figure 4.8: *Typical increase in weight of the gel after the diffusion experiment for a gel sample containing 35 % P(VdF-HFP), 5 % $LiPF_6$ and 60 % EC-PC. (□) Simulated data, sample in contact with EC:PC (+) Experimental data, sample in contact with EC:PC (x) Experimental data, sample in contact with 1 mol/dm^3 $LiPF_6$ (EC:PC) (o) Simulated data, sample in contact with 1 mol/dm^3 $LiPF_6$ (EC:PC)*

Chapter 5

Characterization Results and Implications

This section summarizes the characterization results from the appended papers and the implications of the results. In the first two sections, characterization results for the liquid and the gel electrolyte are presented. The third section deals with the polarization that occurs in a lithium-ion cell due to mass transport limitations in the liquid electrolyte. In the fourth and final part, a new way to benchmark electrolytes is presented.

5.1 The Mass Transport in the Liquid Electrolyte: $LiPF_6$-EC-EMC

Lithium hexafluorophosphate dissolved in a mixture of ethylene carbonate (EC) and ethyl methyl carbonate (EMC) was characterized with the method explained in chapter 4 in a concentration span from 0.2 to 2 mol/dm^3 $LiPF_6$ at 25 °C. In figure 5.1, the conductivity for this electrolyte is shown as a function of the salt concentration. It was measured with a conductometer. It increases rapidly at low concentration and reaches a maximum around 1.0 mol/dm^3. At higher concentrations, the conductivity decreases again. This type of behaviour is typical of lithium-ion battery electrolytes. Ding *et al.* (26) have reported that the ions become increasingly associated and that the viscosity increases with increasing fractions of salt. As a general rule, the conductivity should increase when the number of free ions is added to the electrolyte. However, since the salt becomes more and more associated at higher concentrations and the viscosity increases, the conductivity starts to decrease at high salt concentrations. The conductivity for this electrolyte is approximately 10 to 100 times lower than a standard water electrolyte (48). However, the electrochemical stability window of water-based electrolytes is limited to the potential window between oxygen and hydrogen evolution, which make them unusable in lithium-ion batteries.

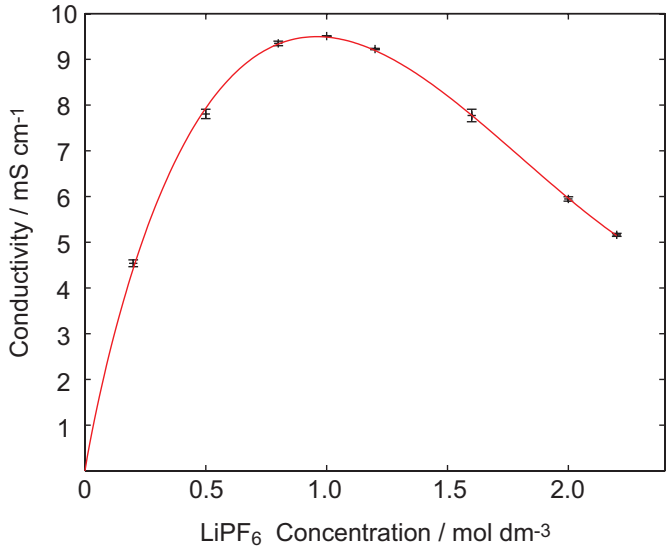

Figure 5.1: *The ionic conductivity of $LiPF_6$ dissolved in EC:EMC with 95 % confidence interval (+) and fitted polynomial (-)*

The salt diffusion coefficient is a measure of the friction forces between the ions and the solvents. In the characterization, it is obtained by optimizing the mass transport model to the experimental data from the galvanostatic polarization experiments. It is plotted as a function of the salt concentration in figure 5.2.

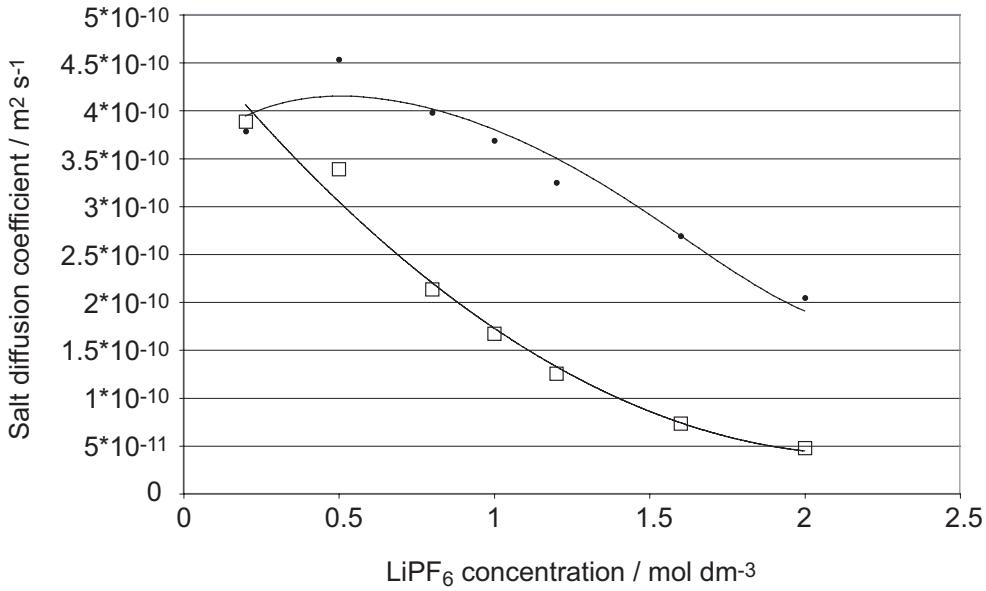

Figure 5.2: *The salt diffusion coefficient of $LiPF_6$ dissolved in EC:EMC.*(□) *Thermodynamic salt diffusion coefficient and* (•) *Apparent salt diffusion coefficient. Fitted polynomials (-) are also shown in the figure.*

It can be defined in two different ways (c.f. table 3.3), either a diffusion coefficient based on the thermodynamic force or an apparent one based on the salt concentration

gradient. The first one describes only the frictions while the second one includes the thermodynamic enhancement factor as well. The first one, the thermodynamic salt diffusion coefficient, decreases with the salt concentration, as a result of the concurrent increase in viscosity and stronger interactions between the solvents and the ions. The second one has a maximum at approximately 0.5 mol/dm^3. The maximum occurs since the thermodynamic enhancement factor and the concentration ratio increases with the concentration while the thermodynamic salt diffusion coefficient decreases.

The lithium ion transport number is a measure of the fraction of the current that is carried by the lithium ions in the absence of concentration gradients. It is obtained from the galvanostatic polarization experiment and it is plotted in figure 5.3. It decreases with the salt concentration, which means that there is a larger increase in the attraction between the solvent and the lithium ions compared to the anion-solvent attractions when the salt fraction increases. Transport number can be defined in different ways. In the figure, it is plotted with respect to the solvent and with respect to the room. The lithium ion transport number with respect to the room is lower than the one with respect to the solvent. At 1.0 mol/dm^3, the values are 0.3 and 0.25 respectively. The anion transport number is equal to one minus the lithium ion transport number, since there are only two ions in the electrolyte that can carry the current. Most of the current is therefore carried by the hexafluorophosphate ion.

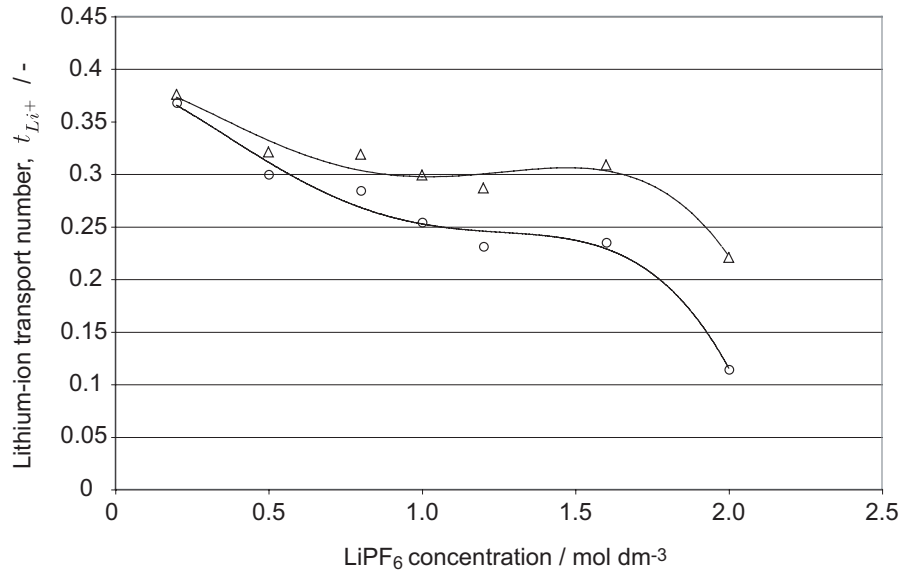

Figure 5.3: *The lithium ion transport number of $LiPF_6$ dissolved in EC:EMC* (△) *Apparent lithium ion transport number with respect to the room and* (○) *Lithium ion transport number with respect to the solvent. Fitted polynomials (-) are also shown in the figure.*

The driving force for the mass transport is dependent on the thermodynamic enhancement factors of the species. In figure 5.4 the thermodynamic enhancement factor of $LiPF_6$ is plotted as function of the salt concentration. The factor can be calculated from η_S when t_+ is known. At low salt concentrations, the factor is approximately one and the electrolyte behaves like an ideal electrolyte. At higher concentrations, the factor increases which increases the driving force for a given

concentration difference (c.f. table 3.2). At 2 mol/dm^3 $LiPF_6$, the thermodynamic enhancement factor is almost 3.5. The thermodynamic enhancement factor of the salt affects the mass transport through D_S and η_S and is thus an important property to take into account at high salt concentrations (c.f table 3.3).

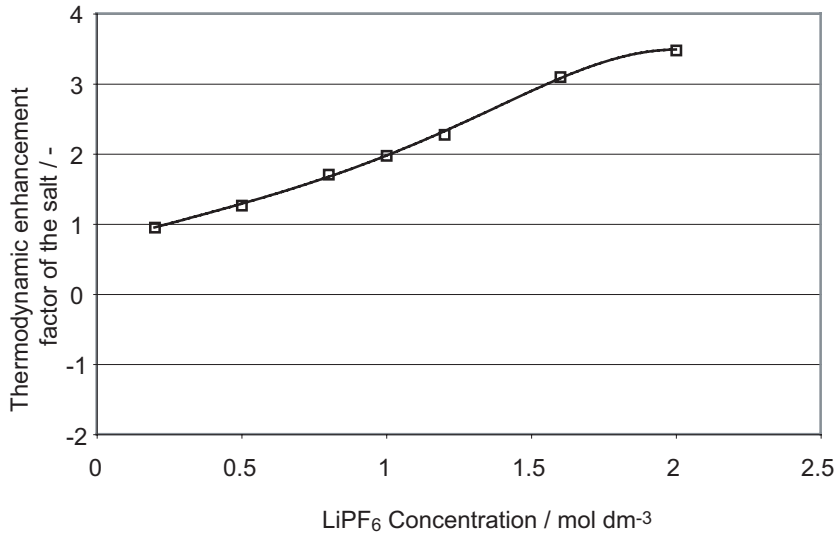

Figure 5.4: *The thermodynamic enhancement factors of $LiPF_6$* (□) *and a fitted polynomial* (-) *of the values.*

The Maxwell-Stefan diffusivities can be calculated from the transport properties and they are plotted in figure 5.5. d_{+-} is lowest, which means that the strongest interaction occurs between the ions. There seem also to be a stronger interaction between the lithium ion and the solvent compared to between the anion and the solvent, which is also indicated in a lithium ion transport number lower than 0.5. At higher concentration, d_{+0} and d_{-0} decrease, which increases the viscosity. The interactions between the ions increase at concentrations higher than 1.2 mol/dm^3 $LiPF_6$, which would suggest that the association of the salt increases at those concentrations.

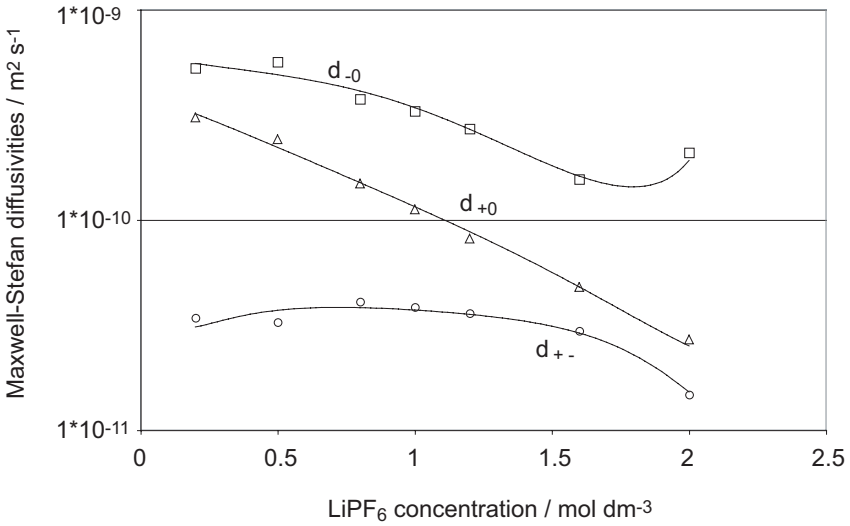

Figure 5.5: *The Maxwell-Stefan diffusivities for the electrolyte $LiPF_6$ dissolved in EC:EMC*

It should be noted that the definitions of the transport properties could differ in the literature. For example, the definition of the lithium ion transport number can change depending on how it is measured. In this thesis, the transport properties are defined according to the Maxwell-Stefan theory and the salt is treated as completely dissociated.

In the optimization of the model, it was found that it was not necessary to use concentration-dependent transport properties, since it did not give better fits, with the exception of η_S that had to be fed into the optimization as a polynomial in concentration. It was also found that there is a slightly larger relative error in the obtained lithium ion transport number compared to the salt diffusion coefficient. The reason for this can be found by studying eq. 4.7. A relative error in the measured diffusion potential would only affect the value of Ψ and thus the lithium ion transport number in an optimization, since such error is not affecting the time dependence of the relaxation. In addition to that, a value of the lithium ion transport number lower than 0.5 would amplify such an error. For example, an experimental relative error of 10 % would lead to a 23 % error in the value of the lithium ion transport number when its true value is 0.3.

5.2 The Mass Transport in the Gel Electrolyte: $LiPF_6$-EC-PC-P(VdF-HFP)

Lithium hexafluorophosphate dissolved in ethylene carbonate (EC), propylene carbonate (PC) and poly(vinylidenefluoride-hexafluoropropylene) (P(VdF-HFP)) has been reported to be a good lithium-ion battery electrolyte with relatively high conductivity (6). The mass transport in this gel was completely characterized with the method described in chapter 4 and the result is presented here.

The conductivity of this gel is seen in figure 5.6. It was measured with electrochemical impedance spectroscopy.

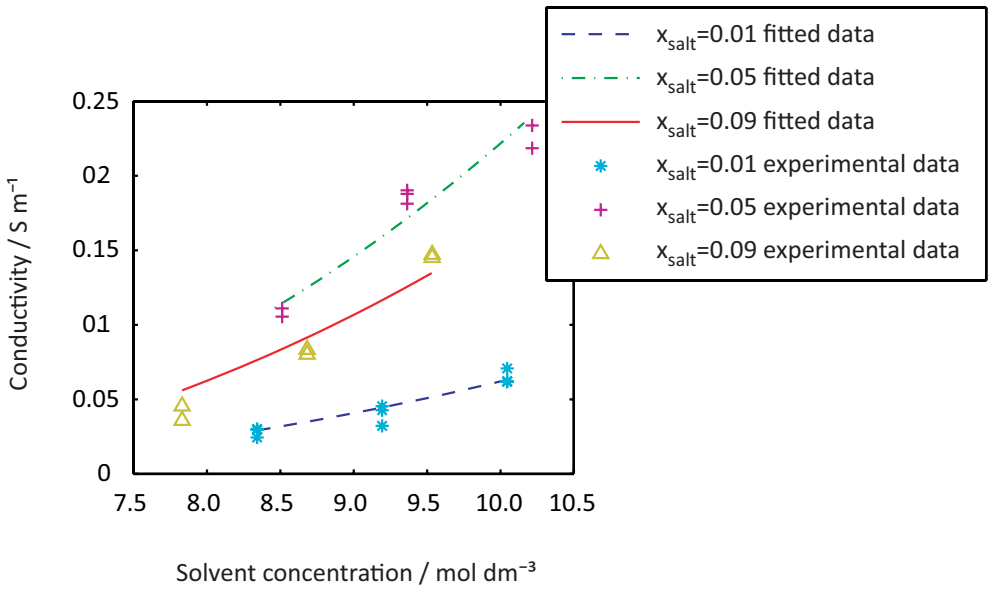

Figure 5.6: *The conductivity of $LiPF_6$ dissolved in EC, PC and P(VdF-HFP) as function of the solvent concentration for different salt fractions.*

As for the liquid electrolyte, the conductivity is a measure of the magnitude of the interactions between the ions and between the ions and the rest of the molecules. The conductivity of the gel shows almost the same type of behaviour as for the liquid (figure 5.1) within the investigated concentration range, except that the conductivity is approximately four times lower. The conductivity increases with the addition of salt and then it decreases, probably due to association and increased interactions between the ions and the solvent and polymer at higher salt concentration. For a fixed salt concentration, the conductivity increases with the solvent concentration, i.e. with decreasing polymer composition. This is expected since the effective dielectric constant increases and the viscosity decreases with the addition of solvent and consequently the conductivity increases. The data show similar trends and values as those reported by Doyle *et al.* (49) for a similar gel. From interpolation of the data, it could be seen that the maximum value of the conductivity occurs for a salt fractions of 0.065.

The lithium ion and solvent transport number are plotted in figure 5.7. The lithium ion transport number is a measure of the fraction of the current that is carried by the lithium ion in the absence of concentration gradients. For a gel that contains 1 % $LiPF_6$ and 40 % P(VdF-HFP), the value is approximately 0.4, which is comparable to lithium ion transport numbers measured for the liquid electrolyte in paper I. For gels with higher salt and polymer concentrations the value of the transport number decreases, which is equivalent to either that the interactions between the lithium ions and the noncharged molecules increase or the interactions between the anion and the noncharged molecules decrease. As seen in the figure, the apparent lithium ion transport number is negative for high salt concentrations. The reason for the negative values is not clear. However, one reason for it could be that there is a large convective flux of the salt in the opposite direction of the current. This flux increases the concentration difference over the electrolyte and is seen in the low apparent lithium ion transport number. The convective flux would be larger for higher salt concentrations,

which agrees with our results. The solvent transport number is positive for all concentrations. It is non-zero, since the interactions between the ions and the solvents give rise to a solvent flux when the current is flowing through the gel.

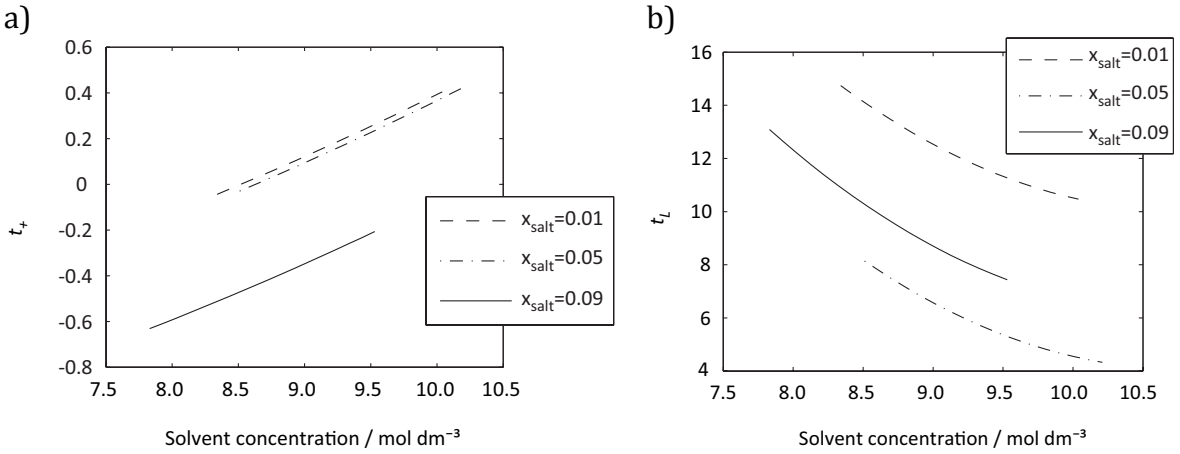

Figure 5.7: *a) The lithium ion transport number and b) the solvent transport number as a function of the solvent concentration for different fractions of salt.*

The diffusion coefficients are plotted in figure 5.8 and 5.9. D_{SL} is not plotted, since the value of it was found to be close to zero in the optimization and the simulated response was not changed when it was set to zero. The fluxes of the lithium ion and the anion are thus independent of the gradient of the solvent concentration. D_{SS} and D_{LL} were found to be positive, as expected.

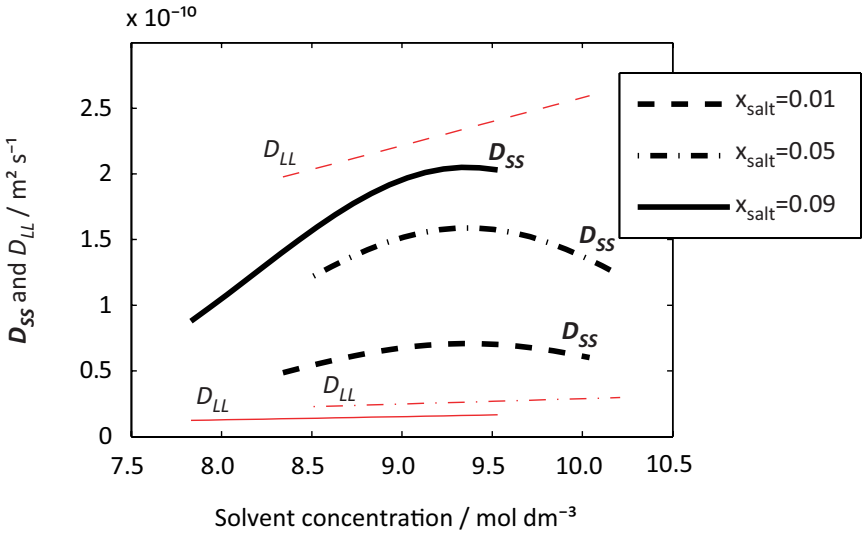

Figure 5.8: *DLL and DSS as a function of the solvent concentration for different fraction of salt.*

D_{LS} was found to be negative, which is expected, since in the diffusion experiments, the mass of the gel increases less for higher concentration of $LiPF_6$ in the liquid electrolyte, which indicated that either D_{SL} or D_{LS}, or both are negative.

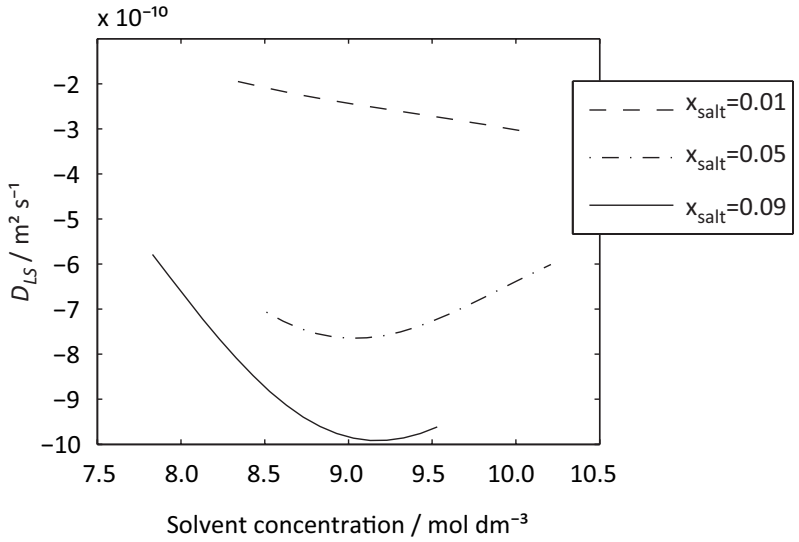

Figure 5.9: *D_{LS} as function of the solvent concentration for different fraction of salt*

The relation between the electrochemical potential and the composition of a gel is measured in concentration cell measurements. It is plotted in figure 5.10. The potential increases with both salt and solvent concentration, although the salt dependence is by far the strongest. The increase of the potential with the polymer concentration indicates interactions between the polymer and the other species in the gel.

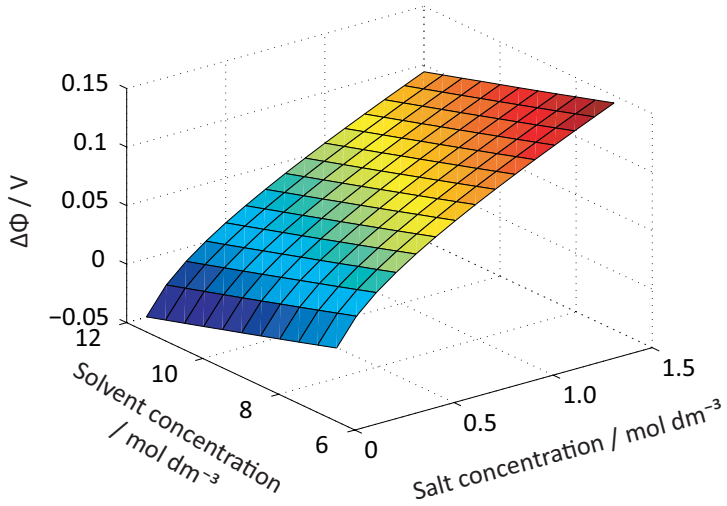

Figure 5.10: *The concentration dependence of the electrochemical potential in the gel measured with a lithium reference electrode. The potential is referenced to a potential of a gel with c_S=100 mol/m³ and c_L= 8900 mol/m³*

η_S and η_L are calculated from the surface in the figure, by talking the derivates of the potential with respect to the salt and solvent concentrations. Their expressions are given in eqs 5.1 and 5.2.

$$\eta_S = 5.326 \cdot 10^{-5} + 2.470 \cdot 10^{-2} \cdot \frac{1}{c_S} \tag{5.1}$$

$$\eta_L = -5.394 \cdot 10^{-6} - 3.616 \cdot 10^{-2} \cdot \frac{1}{c_L} \tag{5.2}$$

We wanted to investigate how large effect a relative error in each of the experimental parameters (η_S, η_L, Ψ_1, Ψ_2, D_1, D_2, Ω_S, and Ω_L) (c.f. eq. 4.9 and 4.10) would have on the apparent transport properties. Relative errors of 1 % were inserted one by one in each of the values of the parameters and the transport properties were calculated from each set of values. The transport properties were calculated with the equations in chapter 4. A relative error in Ψ_1 or Ψ_2 is equivalent to a relative error in the experimentally measured diffusion potential, while a relative error in D_1 or D_2 would for example correspond to a relative error in the measurement of the thickness of the cell. A relative error in η_S, η_L, Ω_S, and Ω_L are equivalent to an error in the measured potential and mass increase in the respective experiment. The result of the analysis is seen in figure 5.11, the standard values of the experimental parameters were taken from the transport properties in a gel with 5 % $LiPF_6$, 35 % P(VdF-HFP) and 60 % EC:PC (paper IV). D_{SL} is equal to zero, so the second column in table 1 in paper III was used to obtain the expressions for D_1, D_2, s_{12} and s_{21}. The transport property that was most sensitive to an error in the experimental data was the lithium ion transport number. It is most sensitive to D_1 and Ψ_1, but η_S and η_L also have a strong influence upon its value. As can be seen in the figure, the relative error of the lithium ion transport number is almost 10 times greater than the relative error that was introduced in the value of D_1 (1 % rel. error). The effect of a relative error in Ω_L is not seen in the figure since there exist only seven independent experimental parameters when D_{SL} is zero. As expected, errors in the values of η_S, η_L, Ψ_1 and Ψ_2 do not affect the values of diffusion coefficients. As a conclusion, the transport numbers is considerably more sensitive to an experimental error than the diffusion coefficients.

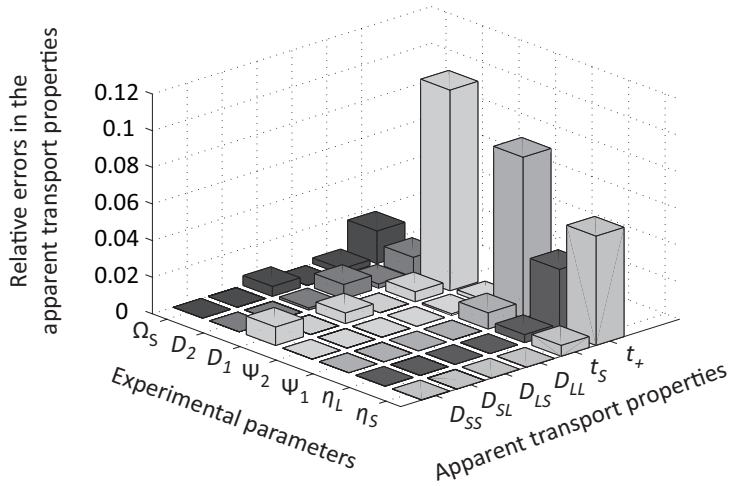

Figure 5.11: *Sensitivity analysis of the characterization method for gel electrolytes*

5.3 Polarization due to the Mass Transport in a Battery Cell

Electrolytes with low lithium ion transport numbers and diffusion coefficients cause large diffusion polarizations during operation of Li-ion battery cells, which lead to poor high-rate performance. The contribution of the diffusion polarization to the total polarization is dependent on the thermodynamic and kinetic material properties, the battery cell design, and how the cell is charged/discharged. To explain and understand the complex behaviour of the polarization in detail, and in particularly the influence of the mass transport, mathematical modelling of the cell can be used. The battery cell, $LiNi_{0.8}Co_{0.15}Al_{0.05}O_2$ (NCA) | 1.2 mol/dm^3 $LiPF_6$ EC:EMC (3:7) | MAG-10, was therefore modelled and simulated during some hybrid pulse power characterization (HPPC) tests defined according to different organizations (c.f. figure 3.2). The electrolyte in the cell was characterized in paper I, while the electrodes have been characterized by Mellgren *et al.* (45) and Brown (44) and these values were used in the model. The result was then analyzed with the method explained in chapter 3.6. The experimentally measured and simulated cell voltage of the cell during a HPPC test defined according to EUCAR are shown in figure 5.12 together with the C-rate and the equilibrium cell voltage.

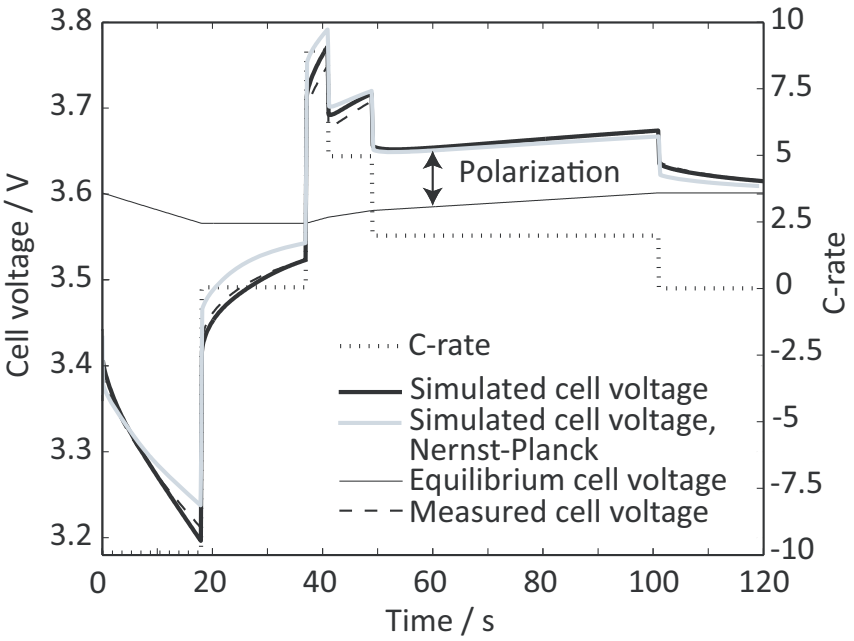

Figure 5.12: *Cell voltage (left axes) and C-rate (right axes) as a function of time during a EUCAR cycle. The polarization is the distance between the cell voltage and the equilibrium cell voltage.*

In the development of the model, several other versions of the model were also tested and compared to the experimental data to determine the necessary extent of details and some valuable conclusions were drawn. For example, the equations describing the mass transport in the electrolyte were exchanged with the Nernst-Planck equations. The equations neglect the non-idealities and the ion-ion interactions of the electrolyte. For this case the simulated cell voltage could not fit the experiments satisfactorily (see figure 5.12). This can be explained by the number of independent transport properties. Only two independent transport properties are found in the Nernst-Planck equation and

that is not enough for describing the mass transport in the electrolyte. This is also shown in characterization results of the liquid electrolyte where the thermodynamic enhancement factor is not unity, which points out that the non-idealities of the electrolyte cannot be neglected.

In the figure, the polarization is the distance between the cell voltage and the equilibrium cell voltage curves. According to the theory presented in chapter 3, it can be divided into six parts, which are associated with processes that occur inside the battery. The processes that are taken into account in the analysis are listed in table 5.1, the expressions that are used to calculate them are found in table 3.6.

Table 5.1: *Processes that are responsible for the polarization in the cell*

Notation	*Explanation*
Ohmic potential drop solid phase	Polarization due to insufficient electronic conductivity in the solid phase of the electrodes
Activation overpotential	Polarization due to activations of the electrochemical reactions
Diffusion polarization solid phase	Polarization due to concentration gradients in the solid phase of the electrodes
Ohmic potential drop electrolyte	Polarization due to insufficient ionic conductivity in the electrolyte
Diffusion polarization electrolyte	Polarization due to concentration gradients in the electrolyte
Contact resistance	Polarization due to inadequate contact between the phases and materials in the electrodes

Figure 5.13 a-b shows a selection of some inner variables from the simulation of the HPPC cycle defined according to EUCAR (figure 3.2a).

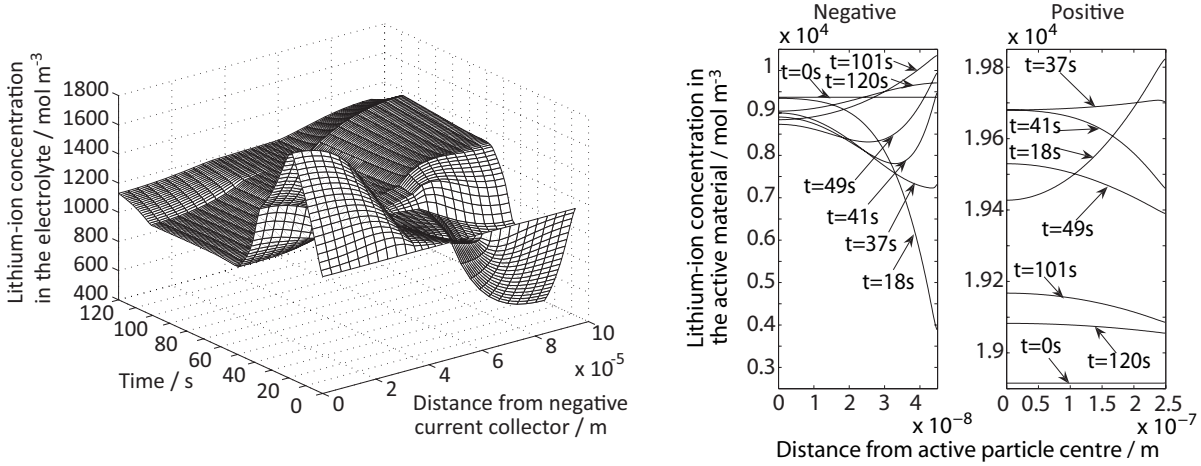

Figure 5.13: *Lithium ion concentration in the a) electrolyte and in the b) active material during a EUCAR cycle*

The lithium ion concentration in the electrolyte is shown in figure 5.13a and the lithium ion concentration in the active material at a point one-third of the electrode length from the separator is shown in figure 5.13b. A difference in the lithium ion concentrations in the electrolyte is built up during both charging and discharging. During the open-circuit periods, the concentration profiles relax towards an even concentration profile. The same occur inside the active materials, where a concentration difference is built up between the inner core and the surface of the particles. Large spatial variations in the lithium ion concentration are seen in both the electrolyte and the active material in the negative electrode during this cycle. Such large concentration differences should lead to mass transport limitations in the cell. This is also seen when the cycle-averaged polarization is calculated (c.f. eq. 3.21).

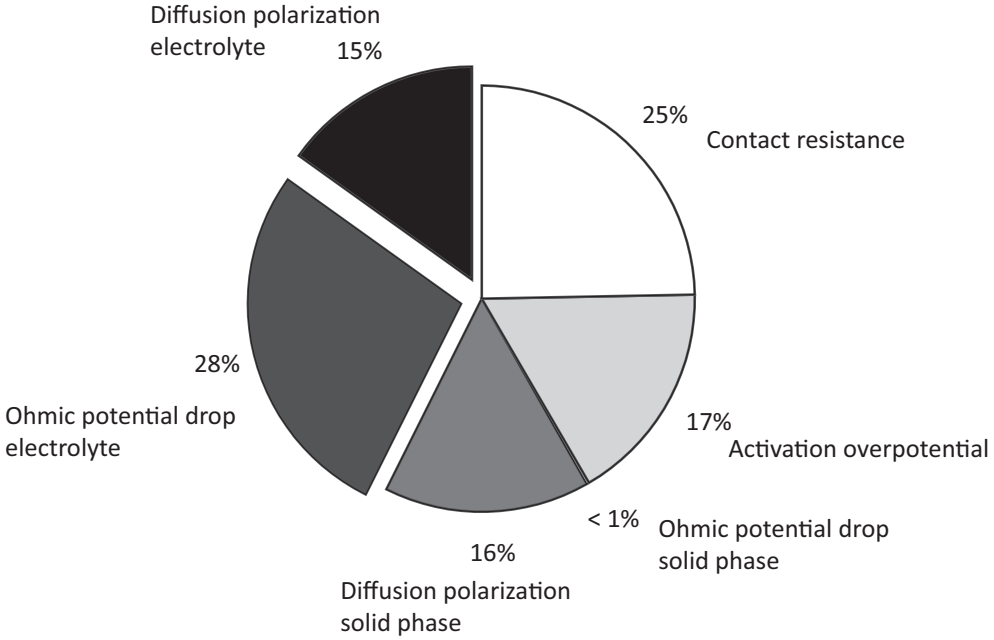

Figure 5.14: *The processes that cause the cycle-averaged polarization when the battery is cycled with a HPPC test defined according to EUCAR. The processes that are associated with the mass transport in the electrolyte are highlighted.*

A pie diagram of the processes that cause the cycle-averaged polarization when the battery is cycled with a HPPC test defined according to EUCAR is seen in figure 5.14. The mass transport in the electrolyte contributes to approximately 43 % of the cycle-averaged polarization, while the concentration differences in the particles (diffusion polarization solid phase) contributes to 16 % of the polarization. The ohmic potential drop in the solid phase is negligible, while the ohmic potential drop in the electrolyte causes a substantial polarization. The contact resistance gives rise to 25 % of the cycle-averaged polarization. The performance of the cell seems therefore to be limited by the insufficient conductivity of the electrolyte and bad contact between the phases in the electrode during this HPPC cycle.

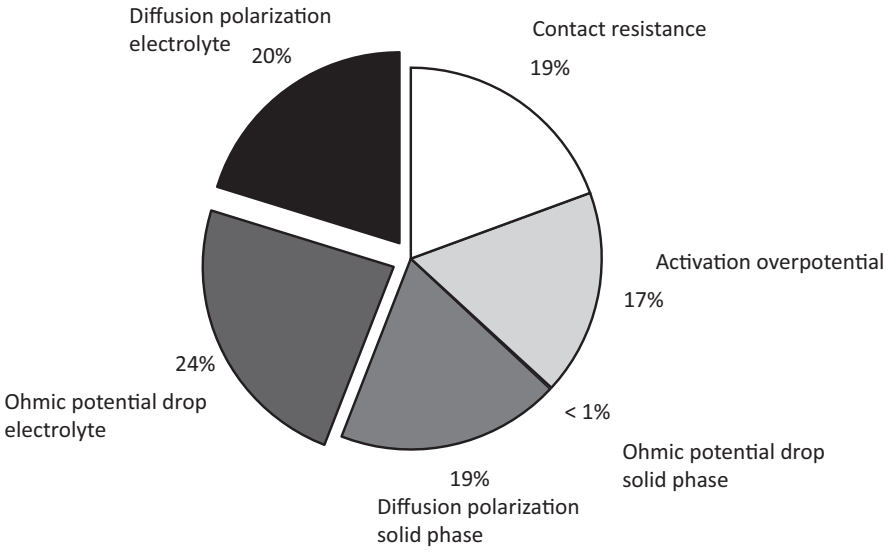

Figure 5.15: *The processes that cause the cycle-averaged polarization when the battery is cycled witg a HPPC test defined according to ISO. The processes that are associated with the mass transport in the electrolyte are highlighted.*

The situation is slightly different for another HPPC test. The split up of the cycle-averaged polarization during a test according to ISO is plotted in figure 5.15. In this test, the mass transport in the electrolyte contributes to 44 % of the polarization. The largest difference between the cycles is that the diffusion polarization in the electrolyte and in the solid phase becomes more important compared to the other processes. The ISO cycle contains higher charge and discharge currents during longer time periods, which increases the concentration differences in the cell.

The importance of the diffusion potential is therefore related to how long the cell is discharged or charged. In figure 5.16, the cycle-averaged polarization for some modified EUCAR cycles is shown. The cycles include the same currents. However, the time for each element has been multiplied with a factor, so that the total time for the cycle is varied.

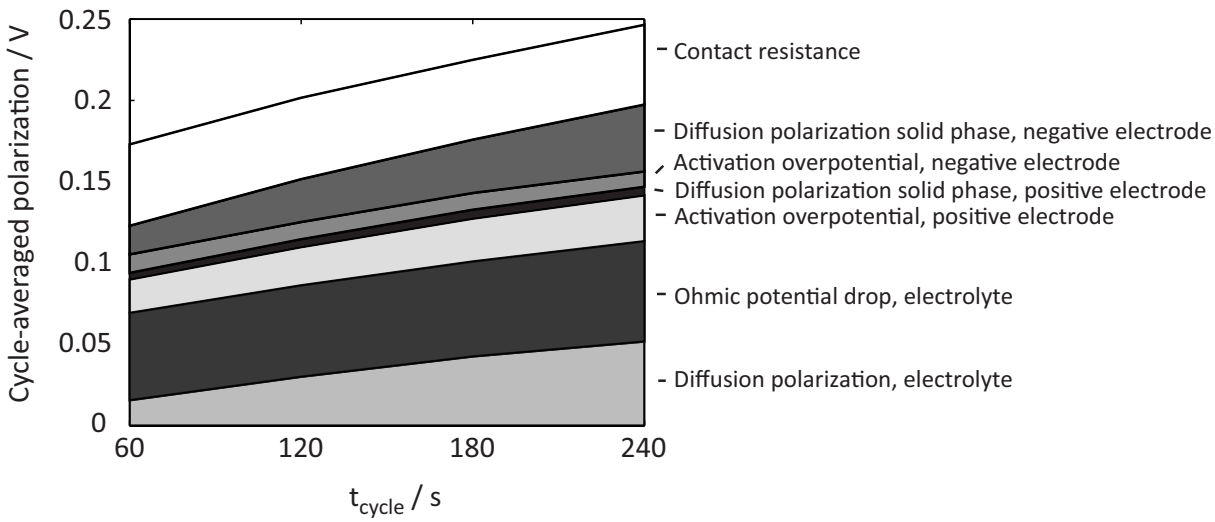

Figure 5.16: *Split up of the polarization during EUCAR cycles of different lengths.*

As can be seen in the figure, the two processes that vary with the total time of the cycle are the diffusion polarization in the electrolyte and in the solid phase of the negative electrode. At t_{cycle}=240 s, the contribution from the diffusion polarization in the electrolyte is almost the same as the contribution from the ohmic potential drop in the electrolyte. The cycle-averaged polarization increases with approximately 50 mV when the time period for each segment in the original cycle is doubled. The increase in the polarization is mainly attributed to an increase in the diffusion polarizations in the electrolyte and the solid phase.

It is not only how the cell is charged or discharged that influence which processes that contribute to the polarization. The geometry of the cell is also important. In figure 5.17, the cycle-averaged polarization during the EUCAR test is plotted as a function of the thickness of the electrodes. The currents in the tests have been modified to correspond to the amount of active material in the electrodes. As the thickness of the electrodes increase, the cycle-averaged polarization increases. The increase is mainly due to an increase in the contact resistance and the ohmic potential drop in the electrolyte. The diffusion polarization increases initially, but stabilizes after 40 µm. The cycle-averaged polarization is strongly correlated to the power density of the battery while the thickness of the electrodes is strongly correlated to the energy density. A high energy-density is achieved by having thick electrodes and a high power density is achieved by a low cycle-averaged polarization. Improving the conductivity of the electrolyte and improving the contact between the phases would therefore increase the energy density without losing any power density.

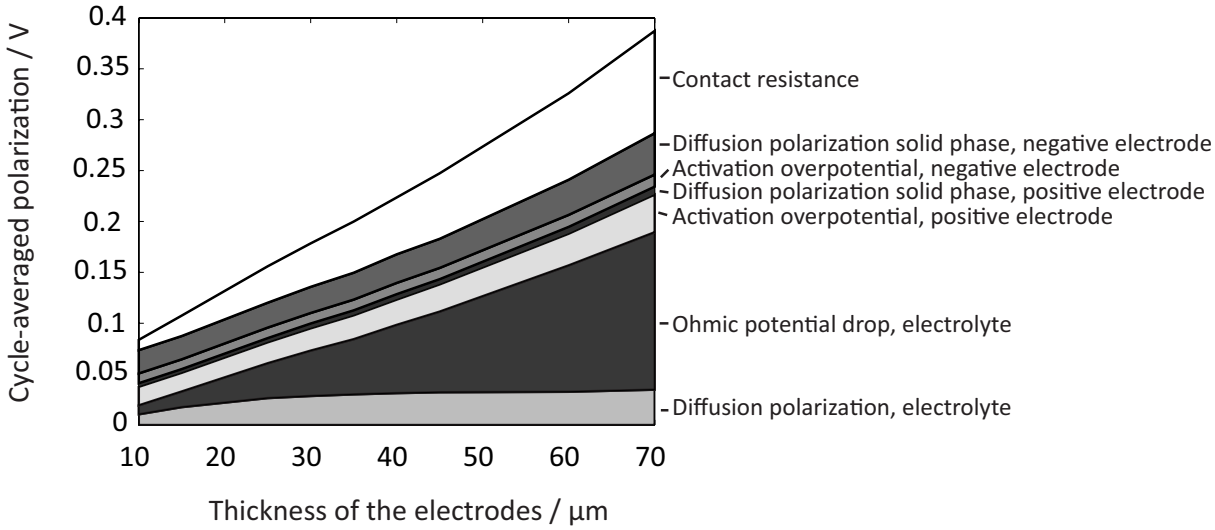

Figure 5.17: *Cycled-averaged polarization for the HPPC cycle defined according to EUCAR for different thicknesses of the electrodes*

5.4 Benchmarking of Electrolytes

There is a need of benchmarking electrolytes in terms of their ability to transport lithium ions with a fast and simple method. The characterizations presented in the previous section are time-consuming and are therefore unsuitable to use as a quick test. Often benchmarking of electrolytes is done by measuring the conductivity alone, since it

is fast and simple. However, as seen in the analysis of the polarization during a HPPC test, the diffusion polarization plays also an important role in the high-power characteristics of a Li-ion battery cell. In paper II and IV, it was suggested that measuring a quantity called the normalized potential gradient should be used as an additional benchmarking test. The normalized potential gradient quantifies the potential drop when the concentration profiles have built up to a steady state. It includes all losses related to limitations in the mass transport, that is both the ohmic potential drop and a term associated with the diffusion potential. It is measured by making a galvanostatic polarization experiment, where the electrolyte is polarized until the concentration profiles have built-up to a steady state. A general equation of the normalized potential gradient is shown in eq. 5.3, where *N* is the number of neutral species in the electrolyte. It is only dependent on the apparent transport properties defined earlier.

$$-\frac{1}{i}\frac{\partial \Phi}{\partial x}\bigg|_{\text{steady state}} = \frac{1}{\kappa} - \frac{1}{i}\sum_{k=1}^{N-1}\eta_k \frac{\partial c_k}{\partial x}\bigg|_{\text{steady state}} \tag{5.3}$$

For a liquid electrolyte, the salt concentration gradient at steady state is given by eq. 5.4.

$$\frac{\partial c_S}{\partial x}\bigg|_{\text{steady state}} = -\frac{(1-t_+)}{D_S}\frac{i}{F} \tag{5.4}$$

By inserting eq. 5.4 in eq. 5.3, the normalized potential gradient can be calculated. It consists of two terms: an ohmic potential drop that is associated with the conductivity and a diffusion potential that is associated with the concentration gradients. In figure 5.18 both the normalized potential gradient and the diffusion potential part (second term in eq. 5.3) are plotted for the electrolyte $LiPF_6$ dissolved in EC:EMC.

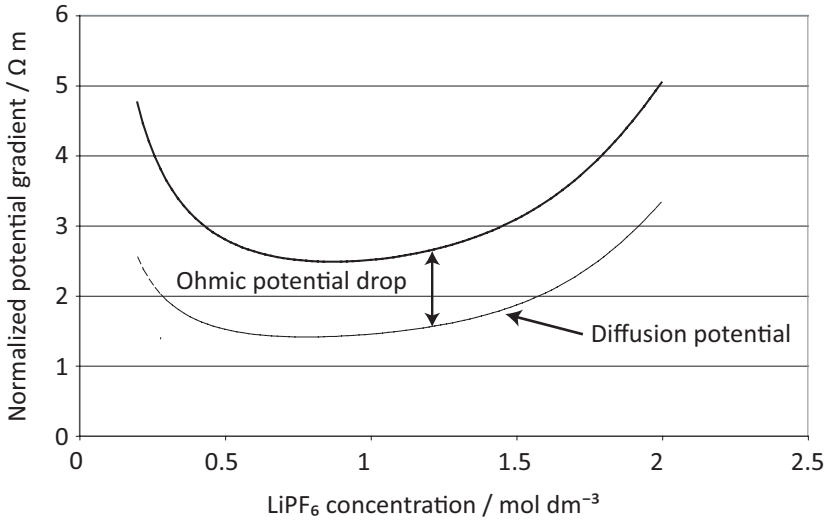

Figure 5.18: *The normalized potential gradient for $LiPF_6$ dissolved in EC:EMC*

The largest contributing part to the normalized potential gradient is the diffusion potential. It increases rapidly at high and low salt concentrations. The minimum value occurs at approximately 0.9 mol/dm^3 $LiPF_6$. However, the normalized potential gradient is quite small in the region 0.5 to 1.2 mol/dm^3 $LiPF_6$.

For a gel electrolyte, the salt and solvent concentration gradients at steady state are given by eqs 5.5 and 5.6 and these equations can be inserted in eq. 5.3 to obtain the normalized potential gradient for gel electrolytes.

$$\left.\frac{\partial c_S}{\partial x}\right|_{\text{steady state}} = -\frac{D_{LL}(1-t_+)+D_{SL}t_L}{D_{SS}D_{LL}-D_{LS}D_{SL}}\frac{i}{F} \tag{5.5}$$

$$\left.\frac{\partial c_L}{\partial x}\right|_{\text{steady state}} = \frac{D_{LS}(1-t_+)+D_{SS}t_L}{D_{SS}D_{LL}-D_{LS}D_{SL}}\frac{i}{F} \tag{5.6}$$

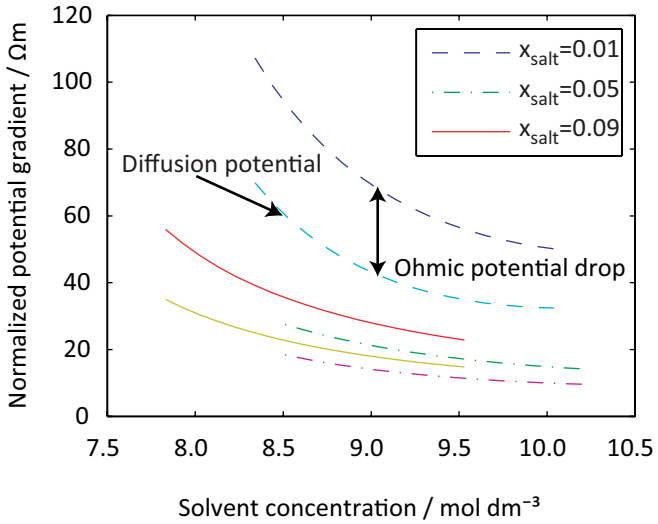

Figure 5.19: *The normalized potential gradient for $LiPF_6$ dissolved in EC:PC and P(VdF-HFP)*

The normalized potential gradient is plotted in figure 5.19 for the gel electrolyte $LiPF_6$ dissolved in EC, PC and P(VdF-HFP). The sum of the diffusion potentials is also here higher than the ohmic potential drop. However, these values are calculated under the assumption that the concentration gradients have had time to build up to a steady state, while at short times the ohmic potential drop is the largest term. To give an example of the time scales in a real battery cell, the concentration gradients reach steady state in approximately 30 seconds in a 50 µm thick gel when a current is passed through and in a liquid electrolyte the process is even faster.

As can be seen in the figure there are large variation in the normalized potential gradient as the fraction of the salt is altered. According to the polynomials that were obtained in the characterization of the gel, the best composition in terms of mass transport would be an electrolyte that contained between 5 and 7 % $LiFP_6$ and as little polymer as possible, without compromising the mechanical stability of the gel. The normalized potential gradient is approximately 15 Ωm at these compositions.

In a battery cell, the liquid electrolyte and the gel electrolyte will fill the pores of the electrodes and the liquid electrolyte will also be soaked into a separator in between the electrodes. The normalized potential gradient will therefore increase, due to the tortuosity and the porosity of the solid materials. This is shown in figure 5.20. The gel electrolyte is better or comparable to the liquid electrolyte in the Celgard separators. However, large values are seen for the gel electrolyte in the electrodes, where the tortuosity and the porosity of the electrodes and the poor mass transport in a gel would increase the polarization in a cell substantially.

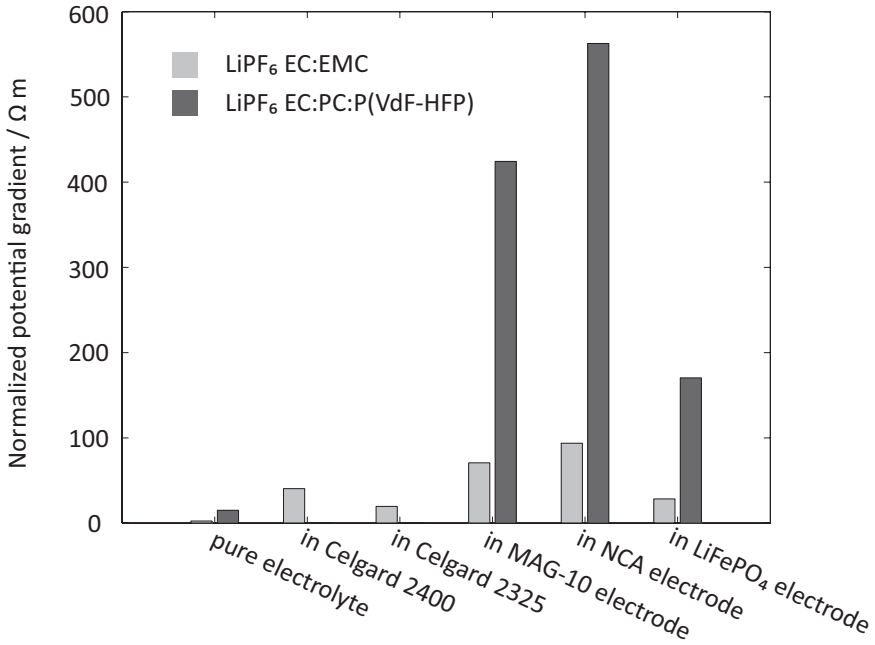

Figure 5.20: *The normalized potential gradient for an optimized composition of the liquid and gelled polymer electrolytes in porous materials. The normalized potential gradients are 2.5 Ωm for the pure liquid electrolyte and 15 Ωm for the pure gel electrolyte. The normalized potential gradient is calculated from the values in table 3.5.*

Chapter 6

Conclusions

The objective of this thesis was to study the mass transport in lithium-ion battery electrolytes. The transport was studied from two perspectives; an electrolyte perspective where the mass transport properties of a liquid and a gel electrolyte were obtained with two characterization methods and a cell perspective where specifically the mass transport in a cell during a hybrid pulse power characterization (HPPC) test was studied. The work involved both experimental work and modelling.

The mass transport was first described by models based on the Maxwell-Stefan equation. From the models, apparent transport properties were identified. The values of the apparent transport properties were then obtained by optimizing the models to the responses of the characterization experiments. A mathematical analysis of the characterization methods was also done in order to establish at which conditions the characterization experiments should be performed.

For the liquid electrolyte $LiPF_6$ dissolved in ethylene carbonate (EC) and ethyl methyl carbonate (EMC); a conductivity, a salt diffusion coefficient, a lithium ion transport number and a thermodynamic enhancement factor describe the mass transport. They were obtained from three different electrochemical experiments, a concentration cell, a galvanostatic polarization experiment and a conductivity measurement. It was found that these transport properties and the model could describe the galvanostatic polarization experiments within the experimental conditions. In the analysis of the characterization method, it was found that the galvanostatic polarizations had to be performed at finite conditions in order to contain information about both the transport number and the salt diffusion coefficient. The concentration gradients that were formed close to the electrodes needed therefore to have time to diffuse into the centre of the electrolyte.

For the gel electrolyte $LiPF_6$ dissolved in ethylene carbonate (EC) and propylene carbonate (PC) and poly(vinylidenefluoride-hexafluoropropylene) (P(VdF-HFP)), nine apparent transport properties were defined from the model. They describe the concentration and potential distribution in an electrolyte where the potential is measured with a lithium reference electrode. The transport properties are one

conductivity, four diffusion coefficients, two transport numbers and two properties that relate a change in the potential to a difference in the composition. To fully characterize a gel electrolyte, the values of all nine properties had be obtained from the characterization experiments. In the characterization, the transport numbers and the diffusion coefficients were obtained from the galvanostatic polarization and the diffusion experiments, while the rest were obtained form the concentration cells and conductivity measurements. Analytical expressions describing the two first experiments were derived and the influence of the properties on the experimental response was investigated. It was concluded that the transport numbers and the diffusion coefficients could be obtained if the model was optimized to results from galvanostatic polarization and diffusion experiments with a sufficiently wide range of experimental conditions. It was especially found that the salt concentration in the liquid during the diffusion experiments and the t_{pol}/L^2 value in the galvanostatic polarization experiments should be varied.

From the concentration dependence of the transport properties of $LiPF_6$-EC-EMC, it could be seen that the interactions between the lithium ions and the solvents increased at higher salt concentrations, which decreased the salt diffusion coefficient. It was also shown that the association of the salt increased at high salt concentrations, which resulted in a decrease in the conductivity. The fit of the models to the experiments was good. It was also found that the characterization method gave a more precise determination of the salt diffusion coefficient than of the lithium ion transport number.

In the characterization of $LiPF_6$-EC-PC-P(VdF-HFP), it was shown that the model could describe the experimental data for a range of conditions and that an optimum set of values of the transport properties could be found that described the experimental data best. A simplified model that treated the polymer and the solvents as one specie and thus contained fewer transport properties could not describe the galvanostatic polarization and concentration cell experiments satisfactorily. One of the diffusion coefficients was equal to zero for this gel, since it was shown that the fluxes of the lithium ion and the anion were independent of the gradient in the solvent concentration. At constant solvent concentration, the conductivity showed an initial increase with the addition of salt followed by a decrease. The lithium ion transport number decreased with the addition of both salt and polymer. All the other transport properties varied with the composition of the gel.

The characterization results of the liquid electrolyte were used in a full cell model of a $LiNi_{0.8}Co_{0.15}Al_{0.05}O_2$ | $LiPF_6$ EC:EMC (3:7) | MAG-10 cell to investigate the mass transport during a HPPC test. In the development of the model, it was found that when the mass transport in the electrolyte was described with the Nernst-Planck equation, the simulated and experimental cell voltages could not be matched satisfactorily. It was therefore concluded from this fact and the characterization results of the electrolyte that the non-idealities and the ion-ion interactions should not be neglected.

An analyzing method was developed to be able to quantify and localize the processes that are responsible for the polarization during current load. The polarization was divided into parts associated with activation of the electrochemical reactions, mass transport of species in the electrolyte and in the solid phase, and inadequate contact between the materials in the electrodes. When the cell was pulsed with a HPPC test

defined according to EUCAR at SOC 40, the polarization arose mainly in the porous electrodes. The mass transport in the electrolyte contributed to approximately 43 % of the polarization during the test. It was found that the diffusion polarization, that is the polarization that arises due to concentration differences in the active material particles and the electrolyte, became more important if the cell was charged or discharged during longer periods without any interruption. If the thickness of the electrodes increased, the polarization increased consequently. The increase was mainly attributed to the ohmic potential drop in the electrolyte and insufficient contact between the phases in the electrodes.

A new method for benchmarking electrolytes was proposed, since complete characterizations are time-consuming and therefore unsuitable to use as screening tests. Measuring a quantity called the normalized potential gradient was therefore proposed as an alternative. It quantifies the potential drop when the concentration profiles in the electrolyte have built up to a steady-state and is thus the sum of the ohmic polarization and the maximum diffusion polarization. The quantity was calculated for the two electrolytes that were characterized previously. The diffusion potential contributed more to the normalized potential gradient than the ohmic potential drop. It was found that the optimum composition for the gel in terms of mass transport was between 5 and 7 % $LiPF_6$ and as little polymer as possible without compromising the mechanical stability of the gel. The optimum composition of the liquid electrolyte was found to lie between 0.5 and 1.2 mol/dm^3 $LiPF_6$.

List of Symbols

a	specific interfacial area / m^{-1}
A	Area of cell or gel disc / m^2
c_i	Concentration / mol m^{-3}
c_k^0	Initial concentration / mol m^{-3}
c_k^{liquid}	Concentration in liquid electrolyte / mol m^{-3}
c_{tot}	Total concentration / mol m^{-3}
d_{ij}	Maxwell-Stefan diffusivity / m^2 s^{-1}
D_{kl}	Apparent diffusion coefficient / m^2 s^{-1}
D_i	Diffusion coefficients in the Nernst-Planck equation
D_k	Apparent diffusion coefficient / m^2 s^{-1}
D_n	Eigenvalues of the diffusion coefficient matrix / m^2 s^{-1}
$\hat{D}_{kl}$	Diffusion coefficient with respect to the polymer / m^2 s^{-1}
f_L, $f_\pm$	Solvent activity coefficient and salt activity coefficient / -
F	Faraday's constant / A s mol^{-1}
F_i	Driving force of the mass transport of component *i* / J m^{-4}
i	Current density / A m^{-2}
I_{pol}	Polarization current / A
j_P	Current density in the pores of the electrodes and separator / A m^{-2}
j_{loc}	Local reaction rate in the electrodes / A m^{-2}
j_{tot}	Total current density defined in paper II / A m^{-2}
L	Thickness of gel disc or electrolyte/ m
N_i	Flux / mol m^{-2} s^{-1}
R	Universal gas constant / J mol^{-1} K^{-1}

$R_{contact}$	Contact resistance / ohm
$R_{electrolyte}$	Electrolyte resistance / ohm
R_d	Radius of gel disc / m
s_{nm}	Substitution parameters defined in table 4.1
t	Time / s
t_c	Contact time / s
t_i	Apparent transport number / -
$\hat{t}_i$	Transport number with respect to the polymer / -
t_{pol}	Time period during which the cell was polarized / s
T	Temperature / K
v_i	Velocity / m s^{-1}
V_m^k	Molar volume / m^3 mol^{-1}
w_k	Parameter in table 4.1
W_1	Weight factor

Greek letters

α	Fitting coefficients defined in paper I and IV
ε	Porosity
γ	Scaling parameter
η_k	Potential diffusion coefficients / V m^3 mol^{-1}
η_{ave}	polarization averaged over a battery domain / V
κ	Conductivity / S m^{-1}
μ_i	Electrochemical potential / J mol^{-1}
μ_i^0	Standard electrochemical potential / J mol^{-1}
σ_{eff}	Effective electronic conductivity / S m^{-1}
τ	Tortuosity
Φ	Quasi-electrostatic potential measured with a lithium electrode / V
Φ_P	Electrolyte potential in the electrolyte / V
Φ_M	Electrolyte potential in the active material / V
Ω_k	Coefficient in eq. 4.10
Ψ	Coefficient in eq. 4.7

Ψ_k	Coefficient in eq. 4.9

Subscript

S	salt
L	solvent
P	polymer
i and *j*	Li^+, PF_6^-, solvent (S) or polymer (P)
k and *l*	salt (S), solvent (L) or polymer (P)
n and *m*	1 or 2

Acknowledgements

I would like to thank my supervisors Mårten Behm and Göran Lindbergh for motivating and supporting me.

The financial support from the Swedish Research Council is gratefully acknowledged.

Thanks to Tommy for valuable cooperation and interesting discussions about modelling. I have enjoyed working with you.

I would also like to thank all present and former colleagues at Applied Electrochemistry.

Ett speciellt tack till Linda för allt stöd du har gett mig; Carina, Lars och alla andra i lunchgruppen för trevligt lunchsällskap; och Kjersti för alla trevliga samtal.

Till sist skulle jag vilja tacka mina nära och kära. Tack för er kärlek och stöd.

References

1. R. Moshtev and B. Johnson, *Journal of Power Sources*, **91**, 86 (2000).
2. I. Buchmann, http://batteryuniversity.com/parttwo-55.htm 20110104, (2005).
3. D. Linden and T. B. Reddy, *Handbook of batteries*, McGraw-Hill, New York (2002).
4. P. G. Bruce, B. Scrosati and J. M. Tarascon, *Angewandte Chemie-International Edition*, **47**, 2930 (2008).
5. J. B. Goodenough and Y. Kim, *Chemistry of Materials*, **22**, 587 (2010).
6. W. A. v. Schalkwijk and B. Scrosati, *Advances in lithium-ion batteries*, Kluwer Academic/Plenum, New York ; London (2002).
7. S. Zhang, T. Jow, K. Amine and G. Henriksen, *Journal of Power Sources*, **107**, 18 (2002).
8. J. S. Newman and K. E. Thomas-Alyea, *Electrochemical systems*, Wiley, Hoboken, N.J. (2004).
9. P. Georén and G. Lindbergh, *Electrochimica Acta*, **49**, 3497 (2004).
10. C. Capiglia, Y. Saito, H. Kageyama, P. Mustarelli, T. Iwamoto, T. Tabuchi and H. Tukamoto, *Journal of Power Sources*, **81-82**, 859 (1999).
11. J. Saunier, W. Gorecki, F. Alloin and J. Sanchez, *Journal of Physical Chemistry B*, **109**, 2487 (2005).
12. H. Kataoka, Y. Saito, T. Sakai, S. Deki and T. Ikeda, *Journal of Physical Chemistry B*, **105**, 2546 (2001).
13. N. A. Stolwijk and S. Obeidi, *Electrochimica Acta*, **54**, 1645 (2009).
14. A. Noda, K. Hayamizu and M. Watanabe, *Journal of Physical Chemistry B*, **105**, 4603 (2001).
15. K. Nishikawa, Y. Fukunaka, T. Sakka, Y. Ogata and J. Selman, *Journal of the Electrochemical Society*, **153**, A830 (2006).
16. S. Stewart and J. Newman, *Journal of the Electrochemical Society*, **155**, F13 (2008).
17. P. G. Bruce, M. T. Hardgrave and C. A. Vincent, *Solid State Ionics*, **53**, 1087 (1992).
18. I. Olsen, R. Koksbang and E. Skou, *Electrochimica Acta*, **40**, 1701 (1995).
19. P. G. Bruce and C. A. Vincent, *Journal of Electroanalytical Chemistry*, **225**, 1 (1987).
20. J. Evans, C. A. Vincent and P. G. Bruce, *Polymer*, **28**, 2324 (1987).
21. H. Xie, Z. Y. Tang, Z. Y. Li, Y. B. He, Y. Liu and H. Wang, *Journal of Solid State Electrochemistry*, **12**, 1497 (2008).
22. L. O. Valoen and J. N. Reimers, *Journal of the Electrochemical Society*, **152**, A882 (2005).
23. M. M. Doeff, P. Georén, J. Qiao, J. Kerr and L. C. De Jonghe, *Journal of the Electrochemical Society*, **146**, 2024 (1999).
24. J. Newman and T. W. Chapman, *AIChE Journal*, **19**, 343 (1973).
25. P. Georén and G. Lindbergh, *Electrochimica Acta*, **47**, 577 (2001).

26. M. S. Ding, K. Xu, S. S. Zhang, K. Amine, G. L. Henriksen and T. R. Jow, *Journal of the Electrochemical Society*, **148**, A1196 (2001).
27. M. S. Ding, K. Xu and T. R. Jow, *Journal of the Electrochemical Society*, **152**, A132 (2005).
28. P. Georén, J. Adebahr, P. Jacobsson and G. Lindbergh, *Journal of the Electrochemical Society*, **149**, A1015 (2002).
29. F. Hallberg, T. Vernersson, E. Pettersson, S. Dvinskikh, G. Lindbergh and I. Furo, *Electrochimica Acta*, **55**, 3542 (2010).
30. H. Dai and T. Zawodzinski, *Journal of Electroanalytical Chemistry*, **459**, 111 (1998).
31. Y. P. Ma, M. Doyle, T. F. Fuller, M. M. Doeff, L. C. Dejonghe and J. Newman, *Journal of the Electrochemical Society*, **142**, 1859 (1995).
32. H. Hafezi and J. Newman, *Journal of the Electrochemical Society*, **147**, 3036 (2000).
33. P. Georén and G. Lindbergh, *Electrochimica Acta*, **49**, 3497 (2004).
34. S. Stewart and J. Newman, *Journal of the Electrochemical Society*, **155**, A458 (2008).
35. A. Stephan, *European Polymer Journal*, **42**, 21 (2006).
36. A. M. Stephan, K. S. Nahm, M. A. Kulandainathan, G. Ravi and J. Wilson, *European Polymer Journal*, **42**, 1728 (2006).
37. P. Georén, *Characterisation and modelling of lithium-ion battery electrolytes*, Ph.D. Thesis, KTH, Stockholm (2003).
38. D. Guyomard and J. Tarascon, *Journal of the Electrochemical Society*, **139**, 937 (1992).
39. C. F. Curtiss and R. B. Bird, *Industrial & Engineering Chemistry Research*, **38**, 2515 (1999).
40. R. B. Bird, W. E. Stewart and E. N. Lightfoot, *Transport phenomena*, Wiley, New York (2002).
41. F. Fornasiero, J. M. Prausnitz and C. J. Radke, *Macromolecules*, **38**, 1364 (2005).
42. J. A. Wesselingh and R. Krishna, *Mass transfer in multicomponent mixtures*, p. 329 s., Delft University Press, Delft (2000).
43. K. Patel, J. Paulsen and J. Desilvestro, *Journal of Power Sources*, **122**, 144 (2003).
44. S. Brown, *Diagnosis of the Lifetime Performance Degradation of Lithium-Ion Batteries : Focus on Power-Assist Hybrid Electric Vehicle and Low-Earth-Orbit Satellite Applications*, Ph.D. Thesis, KTH, Stockholm (2008).
45. N. Mellgren, S. Brown, M. Vynnycky and G. Lindbergh, *Journal of the Electrochemical Society*, **155**, A304 (2008).
46. I. Thorat, D. Stephenson, N. Zacharias, K. Zaghib, J. Harb and D. Wheeler, *Journal of Power Sources*, **188**, 592 (2009).
47. T. B. W. G. EUCAR, Specification of Test Procedures for Hybrid Electric Vehicle Traction Batteries, in (1998).
48. C. H. Hamann, A. Hamnett and W. Vielstich, *Electrochemistry*, VCH, Weinheim (1998).
49. M. Doyle, J. Newman, A. S. Gozdz, C. N. Schmutz and J. M. Tarascon, *Journal of the Electrochemical Society*, **143**, 1890 (1996).